CLNS 89/878
January, 1989

Bunched Beam Diagnostics

R. H. Siemann
Newman Laboratory of Nuclear Studies, Cornell University, Ithaca, N. Y. 14853

Table of Contents

Lectures Presented at the Seventh Summer School
on High Energy Particle Accelerators
Fermi National Accelerator Laboratory
August, 1987

Bunched Beam Diagnostics

R. H. Siemann
Newman Laboratory of Nuclear Studies, Cornell University, Ithaca, N. Y. 14853

I. Introduction

There is a remarkable diversity in the field of accelerator physics. Look at the proceedings of any conference. Papers range from Hamiltonian dynamics to the latest improvements of performance in accelerator X to the engineering of specialized equipment. Beam diagnostics is somewhere in the middle of this. Diagnostic instruments make the connection between theories and observations, and the capabilities of these instruments influence strongly our ability to improve performance.

I gave a series of lectures in 1987 on the general topic of "Principles of Beam Observation". The emphasis was on frequency domain analysis of beam generated signals in storage rings, and that is the subject of this paper. The goal is to connect spectrum analyzer observations to what the beam is doing. In addition, understanding beam spectra is essential for understanding coherent effects and instabilities in storage rings, and this is discussed extensively.

There are a number of other reviews that cover some of the same ground;[1] I have learned a great deal from them and recommend them. In addition, there are numerous conference papers and internal reports describing particular instruments. They are invaluable when you have to design and engineer a detector.

Much of this work was performed while I was on sabbatical leave at Fermilab. I want to thank Helen Edwards, Rich Orr, and Leon Lederman for their hospitality and for the opportunity to work on the Tevatron. I have benefitted from discussions with and working with Gerry Jackson, Marv Johnson, Quentin Kerns, Don Martin, Bob Meller, and Joe Zurawski. Thanks to each of you!

This work was supported in part by the National Science Foundation and the Department of Energy.

---

1. R. Littauer, AIP Conf. Proc. **105**, 869 (1983).
D. Boussard, "Schottky Noise and Beam Transfer Function Diagnostics", Proc. CERN Accel. School, Advanced Accel. Physics, CERN 87-03 (CERN, 1987).
G. Lambertson, AIP Conf. Proc. **153**, 1413 (1987).

II. Signals From Longitudinal Motion

A. Introductory Remarks

It is natural to consider beam diagnostics and beam dynamics in the frequency domain. Particles in a storage ring can be thought of as oscillating in potential wells formed by the magnetic lattice in the transverse and the accelerating fields in the longitudinal. An extremely useful first approximation is that the oscillation frequencies are independent of amplitude, and these frequencies, the tunes, are among the most basic accelerator parameters. Departures from this first approximation are also well described in the frequency domain. Cubic and higher order contributions to the potentials show up as tune spreads, and collective phenomena can be analyzed as perturbations of the basic motion. For these reasons this discussion concentrates on frequency domain analysis and measurements.

Fourier transformations are used for changing between time domain and frequency domain functions. If f(t) is a time domain function, then the convention used in this paper for the Fourier transform, F(ω), is

$$F(\omega) = \int_{-\infty}^{\infty} f(t)\, e^{-j\omega t}\, dt \qquad (1)$$

where $j = \sqrt{-1}$. The inverse transformation is

$$f(t) = \frac{1}{2\pi}\int_{-\infty}^{\infty} F(\omega)\, e^{j\omega t}\, d\omega \qquad (2)$$

Angular frequencies, ω, are the appropriate mathematical variables. However, spectrum analyzers read-out frequencies, $\nu = \omega/2\pi$, and when discussing measurements, these are more convenient quantities. In this paper the word "frequency" depends on context, but formulae keep the distinction between ω and ν-when ω appears, it is always an angular frequency. Unique subscripts denote different physical frequencies, and the subscripts are the same whether referring to frequency or angular frequency. For example, ν_r and $\omega_r = 2\pi\nu_r$ both refer to the rotation frequency.

B. Single Particles

1. Constant Revolution Frequency: Consider a single, unit-charge particle with a constant revolution frequency ω_r (figure 1a). At some azimuth of the machine there is a detector that measures the beam current which is

$$i(t) = \sum_{n=-\infty}^{\infty} \delta(t - nT) \qquad (3)$$

where $T = 2\pi/\omega_r$ is the revolution period. Taking the Fourier transform

$$I(\omega) = \sum_{n=-\infty}^{\infty} \int_{-\infty}^{\infty} \delta(t - nT)\, e^{-j\omega t} = \sum_n e^{-j\omega nT} = \sum_n \exp(-j\, 2\pi n\omega/\omega_r). \qquad (4)$$

The last sum can be thought of as an infinite sum of phasors of unit magnitude that will add up to zero unless all of the phasors are in phase, i.e. unless ω/ω_r is equal to an integer.

Formally this follows from the Poisson Sum Rule[1] which states that if F(ω) is the Fourier transform of f(t), then

$$\sum_{n=-\infty}^{\infty} f(\alpha n) = \frac{1}{\alpha}\sum_{n=-\infty}^{\infty} F\left(\frac{2\pi n}{\alpha}\right) . \qquad (5)$$

Taking $f(t) = \exp(-j\omega t)$ and $\alpha = 2\pi/\omega_r$ gives $F(2\pi n/\alpha) = 2\pi\delta(\omega + n\omega_r)$ and eq. (4) becomes

---

1. P. M. Morse and H. Feshbach, Methods of Theoretical Physics (New York: McGraw-Hill Book Company, 1953) p. 483.

$$I(\omega) = \omega_r \sum_{n=-\infty}^{\infty} \delta(\omega - n\omega_r) . \qquad (6)$$

$I(\omega)$ is a series of δ-functions at $\omega/\omega_r = n$ where n is an integer; this is in agreement with the qualitative argument above. The spectrum is a comb of lines at the rotation harmonics - frequencies that are integer multiples of the revolution frequency (figure 1b).

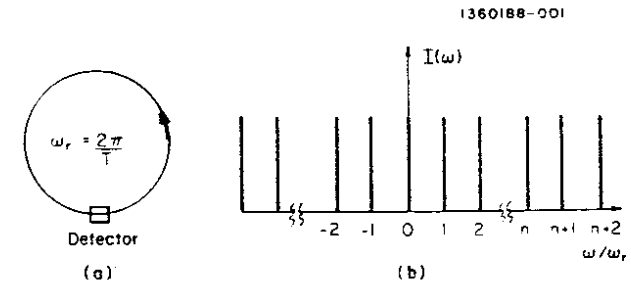

Figure 1: a) A single particle with constant revolution frequency passing a detector once per turn. b) The spectrum of the current measured in the detector.

2. Bunched Beams: In a machine where the beam is bunched by the accelerating fields of an RF cavity the expression for the beam current must include the effects of synchrotron oscillations. In this case the current, i(t), is given by

$$i(t) = \sum_{n=-\infty}^{\infty} \delta(t - nT - \tau_a \cos(\omega_s nT + \phi)). \qquad (7)$$

In this equation T is the revolution period of a synchronous particle, τ_a in the amplitude of the synchrotron oscillation, ω_s is the synchrotron oscillation frequency, and φ is the phase of the oscillation. Taking the Fourier transform

$$I(\omega) = \sum_{n=-\infty}^{\infty} \exp\{-j\omega(nT + \tau_a \cos(\omega_s nT + \phi))\}. \qquad (8)$$

Before proceeding formally, a central feature of this expression, the correlation between the amplitude envelope and the frequencies of the spectral lines, can be seen by Taylor expanding eq. (8)

$$I(\omega) = \sum_{n=-\infty}^{\infty} \exp(-j\omega nT)\left(1 - j\omega\tau_a \cos(\omega_s nT + \phi) - \frac{(\omega\tau_a)^2}{2}\cos^2(\omega_s nT + \phi) + \ldots\right)$$

$$= \sum_{n=-\infty}^{\infty} \exp(-j\omega nT)\left(1 - \frac{(\omega\tau_a)^2}{4} - j\omega\tau_a \cos(\omega_s nT + \phi) + \frac{(\omega\tau_a)^2}{4}\cos\{2(\omega_s nT + \phi)\} + \ldots\right) \qquad (9)$$

When $\omega\tau_a \ll 1$ this reduces to eq. (4); the spectrum is a comb of lines at the rotation harmonics. As $\omega\tau_a$ increases the linear term becomes important, and $I(\omega)$ equals

$$I(\omega) = \sum_{n=-\infty}^{\infty} \exp(-j\omega nT) - j\frac{\omega\tau_a}{2}\sum_{n=-\infty}^{\infty}\Big\{ \exp\{-j((\omega-\omega_s)nT-\phi)\}$$

$$+ \exp\{-j((\omega+\omega_s)nT+\phi)\}\Big\} + \ldots \qquad (10)$$

The new terms are combs of lines offset from the rotation harmonics at $\omega = n\omega_r + \omega_s$ and $\omega = n\omega_r - \omega_s$. These lines have an amplitude envelope that is linear in $\omega\tau_a$ and, therefore, didn't appear when $\omega\tau_a << 1$. For $\omega\tau_a$ large enough that the quadratic term must be considered, there are two more combs at $\omega = n\omega_r + 2\omega_s$ and $\omega = n\omega_r - 2\omega_s$. In addition, the comb at the rotation harmonics decreases in amplitude.

Formally, eq. (8) can be rewritten so that it can be interpreted in the same way as eq. (6) and figure 1b by using a Bessel function sum[2]

$$e^{jz\cos\alpha} = \sum_{k=-\infty}^{\infty} j^k J_k(z) e^{jk\alpha} . \qquad (11)$$

Substituting this into eq. (8) and using the Poisson Sum Rule

$$I(\omega) = \omega_r \sum_{k=-\infty}^{\infty} (-j)^k J_k(\omega\tau_a) e^{-jk\phi} \sum_{n=-\infty}^{\infty} \delta(\omega + k\omega_s - n\omega_r) . \qquad (12)$$

The spectrum is a double-infinity of lines at $\omega = n\omega_r - k\omega_s$ where $n = -\infty,\ldots,\infty$ and $k = -\infty,\ldots,\infty$.

1360188-002

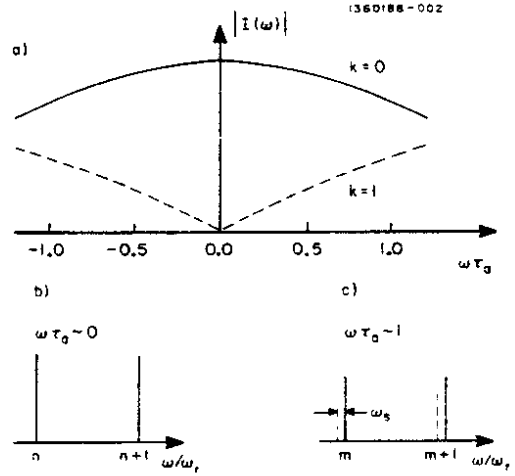

Figure 2: The spectra for k = 0 (solid line) and k = 1 (dashed line). a) The spectral envelopes. b) The spectral lines near $\omega\tau_a \sim 0$; the only lines are for k = 0. c) The lines near $\omega\tau_a \sim 1$; there are both k = 0 and k = 1 lines.

2. I. S. Gradshteyn and I. M. Ryshik, Table of Integrals, Series, and Products (New York: Academic Press, 1965), eq. 8.511.4.

As expected from the discussion above the value of the integer k has consequences for the locations and amplitudes of spectral lines. The lines are sidebands of the rotation harmonics; they are spaced by ω_r and offset from the rotation harmonics by $-k\omega_s$. The factor $J_k(\omega\tau_a)$ determines the envelope of the spectral lines. The first maxima of the Bessel function $J_k(x)$ are approximately at $x = \pm k$. When the magnitude of the argument, $\omega\tau_a$, is substantially less than $|k|$, the envelope factor is small and the sidebands with that value of k have small amplitude. Alternatively, a sideband of a given k can be identified by the offset from a rotation harmonic, and, if such a sideband is prominent, the synchrotron oscillation amplitude must satisfy

1360188-006

$$\tau_a \gtrsim |k/\omega| \qquad (13)$$

where ω is the frequency of observation. Sample spectra for k = 0 and k = 1 are shown in figure 2.

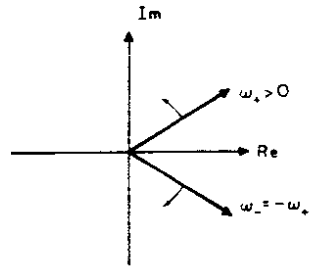

The sum in eq. (12) contains positive and negative frequencies. How does a spectrum analyzer measure negative frequencies? Consider the two phasors shown on the right: one has frequency $\omega_+ > 0$ and the other has frequency $\omega_- = -\omega_+$. The physical quantities represented by these phasors are the projections onto the real axis, and these projections are the same for the two phasors. A spectrum analyzer cannot distinguish positive and negative frequencies!

This has several consequences that are illustrated in figure 3. On the left-hand side of this figure are the "mathematical" spectra given by the δ-functions in eq. (12), and on the right-hand side are the "physical" spectra that would be measured. For k = 0 the measured lines are at $\omega = n\omega_r$ where n = 0,1,2,...; the n = 0 line is one-half the amplitude of the other lines. When the quantity being measured is the beam current, the n = 0 line is 2π times the DC current and all the other lines have an amplitude equal to twice the n = 0 line (4π times the DC current). When $|k| = 1$, the physical spectrum has sidebands spaced $\pm\omega_s$ from the rotation lines, and k = +1 and k = -1 cannot be distinguished. Both k = +1 and k = -1 sidebands appear at the same frequency, and, from eq. (12), the real parts of the currents are in phase. Therefore, the measured current is two times the current from a single sideband. Of course, these remarks hold for all $|k| > 0$.

The envelope in eq. (12) has a factor $\exp(-jk(\phi + \pi/2))$ that gives a phase, but this phase has no meaning for a single particle. For multiple particles the phase takes on substantial significance.

1360188-005

C. Multiple Particles: Introduction

Consider longitudinal phase space with Cartesian coordinates τ, the deviation from the synchronous time, and

$$\varepsilon = -\frac{\alpha}{\omega_s}\frac{\Delta E}{E_0} \qquad (14)$$

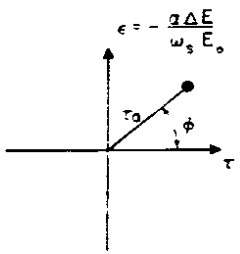

where $\Delta E/E_0$ is the fractional deviation from the nominal energy and α is the momentum compaction. The quantities τ and ε satisfy

$$\tau = \tau_a \cos(\omega_s t + \phi) ,$$

and

$$\varepsilon = \tau_a \sin(\omega_s t + \phi) . \qquad (15)$$

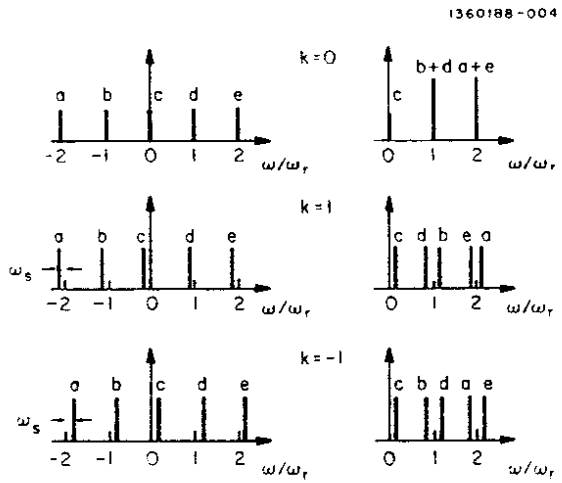

Figure 3: The mathematical (on the left) and physical spectra (on the right) for $k = 0, \pm 1$.

The charge density at $t = 0$ is written as a function of the polar coordinates, τ_a and ϕ where

$$\rho(\tau_a, \phi)\tau_a d\tau_a d\phi = \text{charge in phase space area } \tau_a d\tau_a d\phi. \tag{16}$$

To determine the spectrum of the beam the single particle spectrum, eq. (12), is multiplied by ρ and integrated over phase space. For $k = 0$, the rotation harmonics,

$$I_0(\omega) = \omega_r \int_0^\infty \tau_a d\tau_a \int_0^{2\pi} d\phi \rho(\tau_a, \phi) J_0(\omega\tau_a) \sum_{n=-\infty}^{\infty} \delta(\omega - n\omega_r) \ . \tag{17}$$

The comb of lines at integer multiples of the rotation frequency remains, and there is an envelope given by the convolution of the charge density and J_0. The measured current is given by combining the positive and negative frequency currents

$$I_0^{meas}(\omega) = Q\omega_r \delta(\omega) + 2\omega_r \int_0^\infty \tau_a d\tau_a \int_0^{2\pi} d\phi \rho(\tau_a, \phi) J_0(\omega\tau_a) \sum_{n=1}^{\infty} \delta(\omega - n\omega_r) \tag{18}$$

where Q is the total charge of the bunch

For an example, assume that the distribution is uniform in ϕ and Gaussian in τ with an rms bunch length σ_τ

$$\rho(\tau_a, \phi) = \frac{Q}{2\pi\sigma_\tau^2} \exp\{-\tau_a^2/2\sigma_\tau^2\} \ . \tag{19}$$

The resulting spectrum is[3]

$$I_0^{meas}(\omega) = Q\omega_r \delta(\omega) + 2Q\omega_r \exp(-(\omega\sigma_\tau)^2/2) \sum_{n=1}^{\infty} \delta(\omega - n\omega_r) . \tag{20}$$

It is a comb of lines at multiples of the rotation frequency with a Gaussian envelope with an rms width equal to $1/\sigma_\tau$. Measurements at rotation harmonics over a range of frequencies can be used to determine the bunch length; this requires a detector with a bandwidth from a fraction of $1/\sigma_\tau$ to several times $1/\sigma_\tau$.

There are two different physical situations that lead to different interpretations of the spectra for $|k| > 0$. These are:

CASE I - Particles move independently of each other.

CASE II - The motion of each individual particle depends on the other particles in the beam. This situation arises when beam induced electromagnetic fields, wakefields, are important.

In CASE I measurement of the spectra for $|k| > 0$ are measurements of Schottky noise, and in CASE II they are measurements of collecuve effects.

D. CASE I: Schottky Noise

1. Approximate Picture: A beam can be injected into a storage ring in a way such that the charge density has dependence on both τ_a and ϕ. When the beam particles move independently, the ϕ dependence vanishes due to filamentation and/or randomization. Assume that at $t = 0$ this has happened and ρ is a function of τ_a only

$$\rho(\tau_a, \phi) = \frac{1}{2\pi}\rho(\tau_a) \ . \tag{21}$$

For a given k the spectrum is

$$I_k(\omega) = \frac{(-j)^k}{2\pi} \sum_{n=-\infty}^{\infty} \delta(\omega + k\omega_s - n\omega_r) \int_0^\infty \tau_a d\tau_a \int_0^{2\pi} d\phi \ J_k(\omega\tau_a)\rho(\tau_a) e^{-jk\phi} \tag{22}$$

$$= 0 \text{ for } |k| > 0.$$

The integral over ϕ gives this result independent of the form of $\rho(\tau_a)$. Why? Individual particles have current at $\omega = n\omega_r - k\omega_s$, but the phase of the current depends on ϕ when $|k| > 0$ (see eq. (12)). Therefore, when the charge density has no azimuthal structure, the currents of the individual particles cancel leading to the result in eq. (22).

However, if the situation is as stated, the cancellation cannot be complete. The beam is made up of a finite number of particles, and if these particles are independent as assumed, they cannot be positioned such that the cancellation is perfect. If they were, they wouldn't be independent! The calculation of the beam spectrum is the same as other statistical calculations. The particles in the beam are drawn from a parent distribution that satisfies eq. (21). However, they are a finite sample, and the actual beam distribution has fluctuations from the parent distribution. The beam spectrum shows these fluctuations. Since this is a statistical problem, we expect the deviation from eq. (22) to depend on the square root of number of particles. This residual, statistical current is the Schottky Noise of the beam.

The charge density for P particles is

$$\rho(\tau_a, \phi) = q \sum_{p=1}^{P} \delta(\tau_a - \tau_{ap}) \delta(\phi - \phi_p) \tag{23}$$

---

3. I. S. Gradshteyn and I. M. Ryshik, Table of Integrals, Series, and Products (New York: Academic Press, 1965), eq. 6.614.1.

where q is the charge of an individual particle, and τ_{ap} and ϕ_p are the synchrotron oscillation amplitude and phase of particle p. The current is given by substituting this expression for the charge density into eq. (22) and performing the ϕ and τ_a integrals. The result is

$$I_k(\omega) = \sum_{n=-\infty}^{\infty} I_{nk}(\omega)\,\delta(\omega + k\omega_s - n\omega_r)$$

where

$$I_{nk}(\omega) = q\omega_r \sum_{p=1}^{P} J_k(\omega\tau_{ap}) \exp\{-jk(\phi_p + \pi/2)\} \; . \tag{24}$$

For each set of P particles the $I_{nk}(\omega)$'s are different; they depend on the phase space coordinates of the particles. It follows that at a given time the current is unknown because it depends on the particular set of particles in the accelerator. However, over time the particle distribution changes due to filamentation and randomization, and the mean and rms currents are the meaningful quantities. For stationary random variables time averaging and ensemble averaging are equivalent,[4] and the mean and rms values of $I_{nk}(\omega)$ can be determined by averaging over all samples of P particles. This averaging is denoted by <>'s.

The mean value of the current is

$$\langle I_{nk}(\omega)\rangle = q\omega_r \langle \sum_{p=1}^{P} J_k(\omega\tau_{ap}) \exp\{-jk(\phi_p + \pi/2)\}\rangle = 0 \tag{25}$$

because the phase factor averages to zero. This is the same result as eq. (22). The square of the rms current is

$$\langle I_{nk}^2(\omega)\rangle = \frac{1}{2}\langle I_{nk}(\omega) I_{nk}^*(\omega)\rangle$$

$$= \frac{q^2\omega_r^2}{2} \langle \sum_{p=1}^{P} \sum_{s=1}^{P} J_k(\omega\tau_{ap}) J_k(\omega\tau_{as}) \exp\{jk(\phi_p - \phi_s)\}\rangle \; . \tag{26}$$

When averaged, the phase factor is equal to zero for $p \neq s$ and equal to one for $p = s$. This removes one of the sums in the eq. (26), and

$$\langle I_{nk}^2(\omega)\rangle = \frac{q^2\omega_r^2}{2} \langle \sum_{p=1}^{P} J_k^2(\omega\tau_{ap})\rangle \; . \tag{27}$$

As expected, the rms current is proportional to the square root of the number of particles. Rewriting eq. (27) in terms of $\rho(\tau_a)$ from eq. (21)

$$\left(\langle I_{nk}^2(\omega)\rangle\right)^{1/2} = \omega_r \left(\frac{q}{2}\int_0^{\infty} \tau_a d\tau_a \rho(\tau_a) J_k^2(\omega\tau_a)\right)^{1/2} : \quad \omega = n\omega_r - k\omega_s \; . \tag{28}$$

The measured rms current has contributions from positive and negative frequencies. Applying the same reasoning used in section B for a single particle, at any measurement frequency these contributions are in phase for any set of particles. Therefore, the rms measured Schottky current is twice that given by eq. (28)

$$I_{rms}^{meas}(\omega) = \sum_k \sum_n \bar{I}_{nk}(\omega)\,\delta(\omega + k\omega_s - n\omega_r) \tag{29}$$

where $\bar{I}_{nk}(\omega) = 2\left(\langle I_{nk}^2(\omega)\rangle\right)^{1/2}$ and $\omega = n\omega_r - k\omega_s$, $k \neq 0$.

4. G. Dôme, "Theory of RF Acceleration and RF Noise" in Proc. of CERN Accel. School for Colliding Beam Facilities, CERN 84-15 (CERN, 1984).

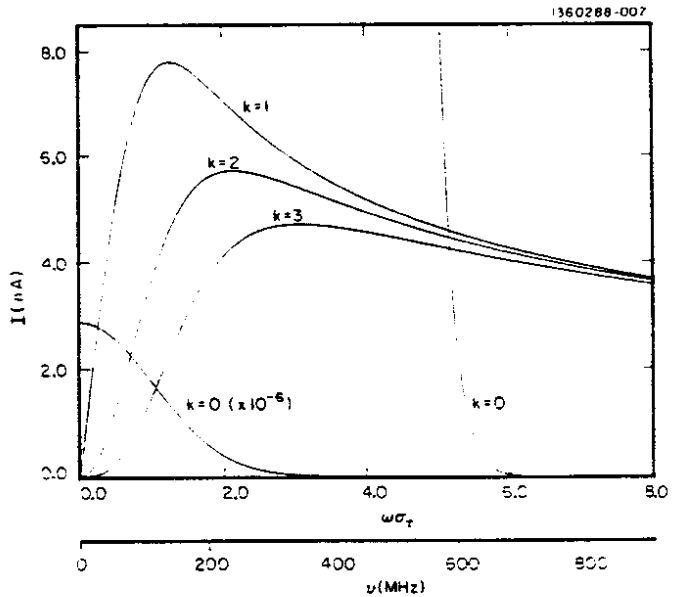

Figure 4: Envelopes of the rotation harmonics (k = 0) and the k = 1, 2, 3 Schottky sidebands for the Tevatron parameters in Table I.

For the Gaussian distribution in eq. (19)[5]

$$\bar{I}_{nk}(\omega) = q\omega_r \left(2P \exp(-\omega^2\sigma_\tau^2) I_k(\omega^2\sigma_\tau^2)\right)^{1/2} \; . \tag{30}$$

where I_k is a modified Bessel function. The envelopes for k = 1, 2, and 3 are plotted in figure 4 (the specific values are for an example that follows). For a given k the envelope has a broad maximum when $\omega \sim k/\sigma_\tau$, and above this frequency it falls off slowly. Integrating over τ_a has washed out all but the first minimum of the J_k's describing the single particle spectra, and the high ω behavior is independent of k.[6] For comparison, the envelope of the rotation harmonics (eq. (20)) is also plotted on the same scale for a beam with $P = 6\times10^{10}$ particles. For $\omega\sigma_\tau = 1$ the current at the rotation harmonics is 2×10^5 times the k = 1 Schottky current, and the Schottky current remains smaller for $\omega\sigma_\tau < 5$.

5. I. S. Gradshteyn and I. M. Ryshik, Table of Integrals, Series, and Products (New York: Academic Press, 1965), eq. 6.633.2.
6. Handbook of Mathematical Functions, edited by Milton Abramowitz and Irene A. Stegun (Washington, DC: U. S. Government Printing Office), eq. 9.7.1.

A measurement of the ratio of the currents at the different sidebands can be used to determine the bunch length. This has the advantage of working in a small frequency range. A resonant, narrowband detector with high sensitivity can be used, and there is no need to correct frequency dependent effects like cable attenuation.

2. Synchrotron Frequency Spread: Up to this point in the discussion, synchrotron frequency spreads have been treated inconsistently to simplify the development of some concepts. Starting at eq. (26) up to eq. (30) it is assumed implicitly that all particles have the same synchrotron frequency, but filamentation was invoked at several points to argue that phase space structure evolves in time. To have such filamentation there must be a spread in synchrotron frequency caused by non-linearities in the RF waveform. The effect of this inconsistent treatment depends on a comparison of the synchrotron frequency spread, $\Delta\nu_s$, and the bandwidth of the spectrum analyzer used for measurements, $\Delta\nu_b$. For a Gaussian density distribution and sideband k, the rms current is given by eq. (30) when $\Delta\nu_b > |k|\Delta\nu_s$.

However, when $\Delta\nu_b < |k|\Delta\nu_s$, the sidebands have a width $|k|\Delta\nu_s$ rather than a unique frequency, and the signal is reduced in amplitude because the number of particles within the bandwidth must be used instead of P. If $\psi(\omega_s)d\omega_s$ is the fraction of particles with synchrotron frequency between ω_s and $\omega_s + d\omega_s$, the rms current is

$$\tilde{I}_{nk}(\omega) = q\omega_r\left(2P\ \Psi_{nk}(\omega)\exp(-\omega^2\sigma_\tau^2)I_k(\omega^2\sigma_\tau^2)\right)^{1/2} \tag{31}$$

where $\Psi_{nk}(\omega)$ is the fraction of the particles in the bandwidth. It is given by

$$\Psi_{nk}(\omega) = \frac{1}{|k|}\int_{\omega}^{\omega+\Delta\omega_b}\psi[(\omega - n\omega_r)/k]\,d\omega\ . \tag{32}$$

The tune spread can be calculated approximately using the method of Kryloff and Bogoliuboff.[7] For a sinusoidal RF voltage the equation of motion is

$$\frac{d^2\tau}{dt^2} + \omega_s^2\tau + \frac{\omega_s^2}{\omega_{RF}}\{\sin(\omega_{RF}\tau) - \omega_{RF}\tau\} = 0 \tag{33}$$

where ω_{RF} is the RF frequency. The last term contains the deviation from a linear restoring force. In the approximate solution the amplitude is unchanged by the non-linearity but the frequency is dependent on the amplitude

$$\tau = \tau_a\cos\{(\omega_s + \Delta\omega(\tau_a))t + \phi\}\ . \tag{34}$$

The quantity $\Delta\omega(\tau_a)$ is given by

$$\begin{aligned}\Delta\omega(\tau_a) &= \frac{\omega_s}{2\pi\omega_{RF}\tau_a}\int_0^{2\pi}\sin\theta d\theta\{\sin(\omega_{RF}\tau_a\sin\theta) - \omega_{RF}\tau_a\sin\theta\} \\ &= -\frac{\omega_s}{2}\left\{1 - \frac{2J_1(\omega_{RF}\tau_a)}{\omega_{RF}\tau_a}\right\}\ .\end{aligned} \tag{35}$$

For a quantitative example consider a single bunch in the Tevatron Collider with parameters given in Table I. The numerical values in figure 4 apply to this example.

1. From eq. (20) the current in a rotation harmonic near $\omega = 0$ is 2.9 mA.

---

7. S. L. Ross, Differential Equations (Waltham, Mass: Blaisdell Publishing Company, 1964), p. 508.

Table I: Longitudinal Motion in the Tevatron Collider, 1987

RF Voltage	$V_{pk} = 1.1 \times 10^6$ V
Beam Energy	E = 900. GeV
Revolution Frequency	$\nu_r = 47.7$ kHz
Harmonic Number	h = 1113
RF Frequency	$\nu_{RF} = h\nu_r = 53.1$ MHz
Momentum Compaction	$\alpha = 0.0030$
Synchrotron Oscillation Frequency	$\nu_s = 37$ Hz
RMS Longitudinal Emittance	$\sigma_\tau\sigma_E = 0.16$ eV-sec
RMS Bunch Length	$\sigma_\tau = 1.4$ nsec
RMS Fractional Energy Spread	$\sigma_E/E = 1.1 \times 10^{-4}$
Number of Particles in a Single Bunch	$P = 6 \times 10^{10}$

2. Using eq. (35) the synchrotron frequency is calculated as a function of oscillation amplitude; the result is shown in figure 5a. The frequency distribution, $\psi(\omega_s)$, for a Gaussian density distribution (eq. (19)) is shown in figure 5b. The synchrotron frequency spread is $\Delta\nu_s \sim 1$ to 2 Hz.
3. Figure 4 shows the comparison of eqs. (20) and (30); the current at the rotation harmonics is greater than the rms Schottky currents out to about 600 MHz where $\omega\sigma_\tau \sim 5$.
4. For $\Delta\nu_b \sim 5$ Hz and small |k|, the sidebands are well separated from each other and eq. (30) is valid. However, caution is advised; when $\omega\sigma_\tau << 5$, the rotation harmonics are so large compared to the Schottky sidebands that it may not be possible to resolve the sidebands.
5. For $|k| \geq 10$ the sidebands overlap. Figure 5c shows the results from eqs. (31) and (32) for $\Delta\nu_b = 1$ Hz and $\omega\sigma_\tau = 6$.

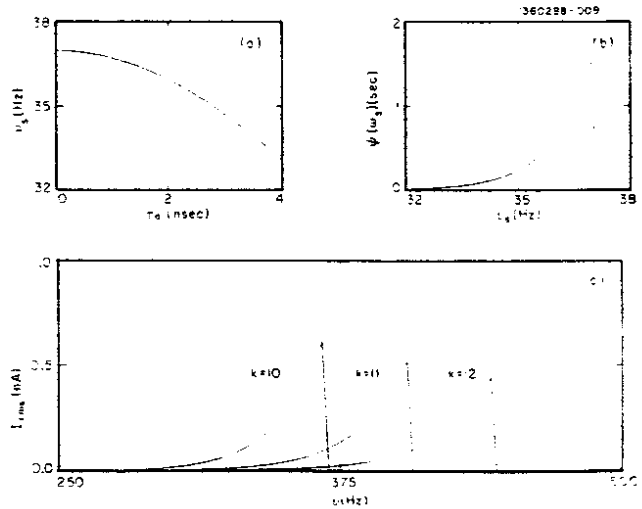

Figure 5: Synchrotron frequency spread in the Tevatron. a) Synchrotron frequency as a function of amplitude. b) Synchrotron frequency distribution. c) Sideband overlap for large k, $\omega\sigma_\tau = 6$

E. CASE II: Collective Effects

In the case of Schottky Noise particles are independent, and signals are due to statistical fluctuations from the average. Particles do not always move independently; they can influence one another through beam generated electromagnetic fields. At high energies the dominant fields, called wakefields, are generated as the beam passes changes in the vacuum chamber profile. When the wakefields are strong, the particles are no longer independent. They act collectively, and the beam develops stable structure in phase space called coherent modes.

A full discussion of collective effects is outside the scope of the present paper; a number of reviews are available.[8] Most theoretical studies of collective effects are done in the frequency domain and use the Fourier transforms of the wakefields which are called impedances. There is an extensive literature devoted to wakefields and impedances, and there are a number of review articles from past accelerator schools with detailed discussions and references to original work.[9]

1. Approximate Picture: For a first approximation assume that there is some stable structure in phase space that rotates with frequency ω_s. The density at time t can be written as a Fourier expansion in ϕ

$$\rho(\tau_a, \phi, t) = \exp(j\omega_s t) \sum_{m=-\infty}^{\infty} \rho_m(\tau_a) \exp(jm\phi) \quad . \tag{36}$$

The quantity $\rho_m(\tau_a)$ is the component with azimuthal periodicity m, and assuming that the structure is stable means that the ρ_m's change slowly compared to measurement time scales. Usually ρ_0 is the dominant term and one or more of the other ρ_m's is non-zero.

The beam spectrum is given by multiplying the single particle spectrum (eq. (12)) by the charge density at t = 0 (eq. (36) with t = 0), and integrating over phase space. For a given rotation harmonic

$$I(\omega) = \omega_r \sum_{k=-\infty}^{\infty} \sum_{m=-\infty}^{\infty} (-j)^k \int_0^{\infty} \tau_a d\tau_a \rho_m(\tau_a) J_k(\omega\tau_a) \int_0^{2\pi} d\phi e^{-j(k-m)\phi}; \tag{37}$$
$$\omega = n\omega_r - k\omega_s \quad .$$

The ϕ integral is equal to zero unless k = m, and, therefore, phase space with azimuthal structure $e^{jm\phi}$ gives spectral lines at $\omega = n\omega_r - m\omega_s$ and signals at $\omega = |n\omega_r - m\omega_s|$. Conversely, a signal at $\omega = n\omega_r - m\omega_s$ ($\omega > 0$) with amplitude greater than the Schottky signal indicates a coherent mode with azimuthal phase space structure $e^{jm\phi}$ or $e^{-jm\phi}$. Since there may be more than one structure in phase space, there can be more than one sideband present.

In contrast to the Schottky case, the signal,

$$I_{nm}(\omega) = \omega_r 2\pi(-j)^m \int_0^{\infty} \tau_a d\tau_a \rho_m(\tau_a) J_m(\omega\tau_a) \qquad (\omega = n\omega_r - m\omega_s), \tag{38}$$

has an arbitrary amplitude because of the proportionality to ρ_m. For a coherent mode with a dominant structure at amplitude τ_a, the signal will be strongest in the frequency range $\omega \sim m/\tau_a$ because of the convolution with J_m; i.e. the signal from a structure of high azimuthal periodicity (large m) will be strong at high frequencies.

---

8. J. L. Laclare, 11th International Conference of High-Energy Accelerators (Basel: Birkhaeuser Verlag, 1980, edited by W. S. Newman), p. 526.
   C. Pellegrini, AIP Conf. Proc. **87**, 77 (1982).
   A. W. Chao, AIP Conf. Proc. **105**, 353 (1983).
   J. M. Wang, AIP Conf. Proc. **153**, 697 (1987).
9. R. H. Siemann, AIP Conf. Proc. **127**, 368 (1985).
   K. Bane, T. Weiland and P. Wilson, AIP Conf. Proc. **127**, 875 (1985).
   B. Zotter, AIP Conf. Proc. **153**, 663 (1987).

2. Coherent Tune Shifts: In writing eq. (36) frequency shifts due to wakefields were neglected. This simplification leads to the relationships between signal frequency, amplitude, and phase space structure (the basic results), but must be modified to account for coherent frequency shifts and instabilities. A more complete expression for the density at time t is

$$\rho(\tau_a, \phi, t) = \exp(j\omega_s t) \sum_{m=-\infty}^{\infty} \exp(jm\phi) \left(\sum_p \rho_{mp}(\tau_a) \exp(j\Delta\Omega_{mp} t) \right) . \tag{39}$$

As in eq. (36), the charge density is expanded in a Fourier series in ϕ. In addition, the ρ_m's are expanded using an appropriate basis; this is symbolized by the summation over p. The resulting modes are characterized by two integers describing the azimuthal and radial (τ_a) structure, m and p, and have phase space rotation frequencies $\omega_{mp} = \omega_s + \Delta\Omega_{mp}$.

Calculation of the mode structures (the ρ_{mp}'s) and frequency shifts (the $\Delta\Omega_{mp}$'s) is the subject of papers on collective effects. Much of the underlying physics in those papers is contained in the discussion above. A mode has an associated current given by a generalization of eq. (37); this current induces a voltage equal to the product of the current and the accelerator impedance summed over all spectral lines. This voltage modifies the beam density distribution, and the problem becomes an eigenvalue problem-finding the phase space distribution consistent with the induced voltage.

A summary of the important results of detailed calculations is:

1. The coherent modes and frequency shifts are solutions of the Vlasov equation. A perturbation approach leads to an integral equation that involves a convolution over frequency of the current and the longitudinal impedance.
2. Approximate solutions for the $\Delta\Omega_{mp}$'s are proportional to the beam current and the longitudinal impedance weighted by a frequency dependence of the mode. As a consequence, the frequency shifts are different for different modes.
3. The $\Delta\Omega_{mp}$'s are complex. The real part, $\Delta\omega_{mp} = \mathrm{Re}(\Delta\Omega_{mp})$, changes the phase space rotation frequency from ω_s to $\omega_s + \Delta\omega_{mp}$. The imaginary part, $\Gamma_{mp} = -\mathrm{Im}(\Delta\Omega_{mp})$, can lead to mode growth or damping; at low beam currents effects such as Landau damping or radiation damping can dominate and prevent instabilities.
4. $\Delta\omega_{mp}$ depends on the imaginary part of the impedance which gives the component of the beam induced voltage that is out of phase with the current.
5. Γ_{mp} depends on the real part of the impedance. This component of the beam induced voltage is in phase with the current, and, therefore, can add or remove energy from a mode.
6. When $|\Delta\Omega_{mp}| \sim \omega_s$, modes can couple leading to an instability (the microwave instability) with large growth rates.

When a coherent mode is stable or the measurement time is long compared to the instability growth time, the signal can be calculated in a way analogous to that leading to eq. (38). The appropriate single particle spectrum is given by eq. (12) with the synchrotron frequency shifted by $\Delta\omega_{mp}$

$$I(\omega) = \omega_r \sum_{k=-\infty}^{\infty} (-j)^k J_k(\omega\tau_a) e^{-jk\phi} \sum_{n=-\infty}^{\infty} \delta(\omega + k(\omega_s + \Delta\omega_{mp}) - n\omega_r) \quad . \tag{40}$$

Multiplying by the charge density of the mode at t = 0, $\rho_{mp}(\tau_a)e^{jm\phi}$, and integrating over ϕ gives the signal

$$I_{nmp}(\omega) = \omega_r 2\pi(-j)^m \int_0^{\infty} \tau_a d\tau_a \rho_{mp}(\tau_a) J_m(\omega\tau_a) \; ; \tag{41}$$
$$\omega = n\omega_r - m(\omega_s + \Delta\omega_{mp}) \quad .$$

This result is essentially the same as eq. (38); the differences are:

1. The need for a third "quantum number", p, to describe the τ_a dependence of the phase space structure of a mode; the ϕ dependence is not a sufficient description.

2. The current of a mode is not necessarily a constant. If the mode is stable it is constant, but it grows with rate Γ_{mp} if the mode is unstable.
3. The oscillation frequency can shift with beam current. Date such as shown in figure 6 for CESR:[10] can give information about the accelerator impedance, but that information is qualitative at best (see the CESR reference for an example). For transverse motion frequency shift measurements are easier to interpret quantitatively, and they are often performed and and the results quoted.

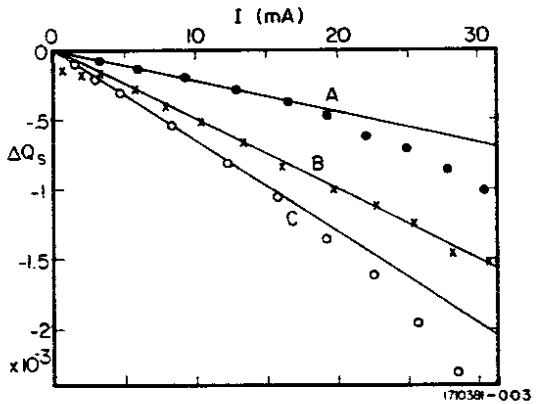

Figure 6: Synchrotron tune shift with beam current in CESR. A, B, & C are for different accelerator conditions.

F. Multiple Particles: Summary

This is a summary of the previous three sections.

Rotation Harmonics

Spectrum — A comb of lines at integer multiples of the rotation frequency, $\omega = n\omega_r$, $n = 0,1,2,...$ (eq. (18))

Envelope — 1. DC ($\omega = 0$) current = $Q\omega_r$. (eq. (18))
2. For a general charge density the envelope is the convolution of the charge density and J_0. (eq. (18))
3. For a Gaussian bunch the envelope is a Gaussian with rms width equal to $1/\sigma_\tau$. (eq. (20))

Measurement — A measurement of the current over a range of frequencies can be used to determine the rms bunch length.

Schottky Noise

Spectrum — For each rotation harmonic a comb of sidebands at integer multiples of the synchrotron frequency, $\omega = n\omega_r + k\omega_s$, $k = -\infty,...-1,1,...\infty$. (eq. (29))

Envelopes — 1. The overall normalization is known; it is proportional to the square root of the number of particles. ((eq. 25))
2. If $\rho(\tau_a)$ is known, the frequency dependence of the rms current is known. There are no relative or absolute uncertainties. (eq. (28))
3. For a general charge density the envelope is a convolution of charge density with J_k^2. (eq. (28))
4. For a Gaussian bunch the envelopes rise from 0 at $\omega = 0$ to a maximum value at $\omega \sim k/\sigma_\tau$ and are approximately independent of frequency above that value. (eq. (30) and figure 6)

Measurement — 1. The sideband frequencies give the synchrotron frequency ω_s.
2. The ratio of the amplitudes of the sidebands in a narrow frequency range gives the bunch length.

Collective Effects

Spectrum — A collective mode with azimuthal dependence $\exp(jm\phi)$ produces sidebands of the rotation harmonics at $m\omega_s$. In addition, there is a frequency shift $\Delta\omega$ that depends on the mode, $\omega = n\omega_r + m(\omega_s + \Delta\omega)$. (eq. (40))

Envelopes — 1. The minimum detectable signal is that due to Schottky noise.
2. The overall normalization is not known. (eq. (38))
3. The frequency dependence is determined by the τ_a dependence of the coherent mode. Signals from coherent modes with high phase space periodicity tend to be strong at high frequencies (eq. (38))

Measurement — 1. A signal above the Schottky noise level is an indication of a coherent mode. The displacement of the sideband from the rotation harmonic gives the azimuthal structure of the mode.
2. Frequency shift as a function of current gives qualitative information about the accelerator impedance.

---

10. D. H. Rice et al, IEEE Trans. Nucl. Sci. NS-28, 2446(1981).

III. Signals From Transverse Motion

A. Introductory Remarks

The signals generated by the transverse motion of particles in a beam can be analyzed with the same techniques. Many of the results are similar, but there are important differences that arise from the dependence of the transverse signal on longitudinal motion.

The beam current is the quantity that is measured in the longitudinal; in the transverse it is the dipole moment

$$d(t) = i(t)x(t) \tag{1}$$

where x(t) is the transverse displacement (from the center of the detector). It has contributions from closed orbit errors, betatron oscillations, and synchrotron oscillations. Begin by considering single particles.

B. Single Particles

1. Constant Revolution Frequency: The dipole moment of unit-charge particle is

$$d(t) = \{X_c + \eta \frac{\Delta E}{E_0} + A_\beta \exp(j\omega_\beta t)\} \sum_{n=-\infty}^{\infty} \delta(t - nT) \ . \tag{2}$$

The first term is from the closed orbit error, X_c, and the second is from the deviation from the nominal energy. η is the dispersion at the detector, and T, the revolution period, depends on $\Delta E/E_0$. The third term is due to a betatron oscillation with amplitude A_β and frequency

$$\omega_\beta = Q_\beta \omega_r = (n_\beta + q_\beta)\omega_r \ . \tag{3}$$

Q_β is the betatron tune, and n_β and q_β are the integer and fractional parts of the tune, respectively. Figure 1a shows d(t); the dark lines are the dipole moment on successive turns. The average value is $X_c + \eta\Delta E/E_0$, and the variations from the average have amplitude A_β.

The Fourier transform is

$$D(\omega) = \{X_c + \eta \frac{\Delta E}{E_0}\} \sum_{n=-\infty}^{\infty} e^{-j\omega nT} + A_\beta \sum_{n=-\infty}^{\infty} e^{-j(\omega - \omega_\beta)nT}$$

$$= \{X_c + \eta \frac{\Delta E}{E_0}\}\omega_r \sum_{n=-\infty}^{\infty} \delta(\omega - n\omega_r) + A_\beta \omega_r \sum_{n=-\infty}^{\infty} \delta(\omega - (\omega_\beta + n\omega_r)) . \tag{4}$$

The closed orbit error and energy deviation lead to lines at the rotation harmonics. This signal is the same as for the longitudinal. The betatron oscillation lines are offset from the rotation harmonics by ω_β. Only the fractional part of Q_β can be determined; nothing depends on n_β because it can be absorbed in index of summation.

Figure 1b illustrates the spectrum. The signals from the closed orbit error and energy deviation are separated from those due to betatron oscillations. The measured spectrum is obtained by combining the positive and negative frequency signals (figure 1c). There are two betatron lines between each pair of rotation harmonics; one of these is the positive frequency line and the other the negative frequency line. There is no way to distinguish them without changing the tune, and q_β derived from the spectrum has an ambiguity between q_β and $1 - q_\beta$. However, the change in signal frequency with a small change in Q_β can resolve the ambiguity.

2. Bunched Beams: Synchrotron oscillations affect the dipole moment in three ways: 1) the arrival time is modulated, 2) the energy deviation is not constant, and 3) Q_β can be energy dependent. The dipole moment is

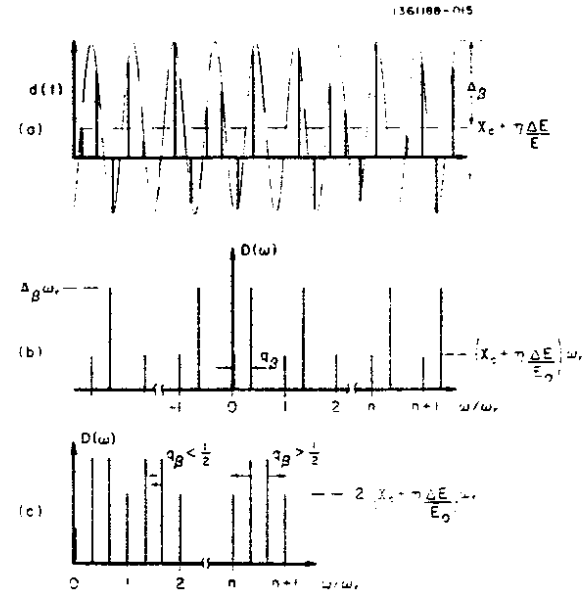

Figure 1: Constant revolution frequency. a) The dipole moment, d(t), on successive turns. b) The spectrum of d(t). c) The measured spectrum. Arrows indicate the directions betatron lines would move if Q_β is increased.

$$d(t) = \{X_c - \frac{\eta\omega_s}{\alpha}\tau_a \sin(\omega_s t + \phi) + A_\beta e^{j\Psi_\beta(t)}\} \times$$

$$\sum_{n=-\infty}^{\infty} \delta[t - nT - \tau_a \cos(\omega_s nT + \phi)] \tag{5}$$

As is eq. (II.7) T is the revolution period of a synchronous particle and τ_a, ω_s and ϕ are the amplitude, frequency and phase of the synchrotron oscillation. The argument of the δ-function accounts for the modulation in arrival time. The three terms in {}'s correspond to the closed orbit error, the variation of the energy deviation, and the betatron oscillation. In the following each is considered separately.

The signal from the closed orbit error is

$$d(t) = X_c \sum_{n=-\infty}^{\infty} \delta(t - nT - \tau_a \cos(\omega_s nT + \phi)) \ . \tag{6}$$

Except for the proportionality to X_c, this is identical to the longitudinal signal given by eq. (II.7). The Fourier transform,

$$D(\omega) = X_c \omega_r \sum_{k=-\infty}^{\infty} (-j)^k J_k(\omega\tau_a) e^{-jk\phi} \sum_{n=-\infty}^{\infty} \delta(\omega + k\omega_s - n\omega_r) \ . \tag{7}$$

is a series of lines offset from the rotation harmonics by multiples of ω_s. The offsets and spectral envelopes are related as they are in the longitudinal.

The signal associated with the energy deviation is

$$d(t) = \eta \frac{\Delta E}{E_0} \sum_{n=-\infty}^{\infty} \delta(t - nT - \tau_a \cos(\omega_s nT + \phi))$$

$$= -\frac{\eta\omega_s}{\alpha} \tau_a \sin(\omega_s t + \phi) \sum_{n=-\infty}^{\infty} \delta(t - nT - \tau_a \cos(\omega_s nT + \phi)) \quad . \tag{8}$$

Equations (II.14) and (II.15) have been used. Taking the Fourier transform and using the Bessel function sum (eq. (II.11)) and the Poisson sum rule (eq. (II.5)) gives

$$D(\omega) = \frac{j\eta\omega_s\tau_a}{2\alpha}\omega_r \sum_k (-j)^k \sum_n \{J_k((\omega - \omega_s)\tau_a) e^{j(k+1)\phi} \delta(\omega - n\omega_r - (k+1)\omega_s)$$

$$- J_k((\omega + \omega_s)\tau_a) e^{j(k-1)\phi} \delta(\omega - n\omega_r - (k-1)\omega_s)\} \quad . \tag{9}$$

Again, the signal is offset from the rotation harmonics by multiples of ω_s, but the relationship between the offsets and envelopes is different than for a closed orbit error.

In particular, synchrotron sidebands appear at low frequencies, $\omega\tau_a << 1$, where the dominant contribution is from $k = 0$. For $1/\tau_a >> \omega >> \omega_s$ the Bessel functions are approximately equal, and

$$D_0(\omega) = \frac{j\eta\omega_s\tau_a}{2\alpha}\omega_r \sum_n J_0(\omega\tau_a) \{e^{j\phi}\delta(\omega - (n\omega_r + \omega_s)) - e^{-j\phi}\delta(\omega - (n\omega_r - \omega_s))\}. \tag{10}$$

This spectrum is a comb of lines offset from the rotation harmonics by $\pm\omega_s$. It is illustrated in figure 2 together with the from a closed orbit error. At higher frequencies there is a similar contrast between the closed orbit and energy oscillation contributions to the signal.

Momentum dependence of the betatron tune produces qualitatively new features in the spectrum from betatron oscillations. The chromaticity, ξ, is defined by

$$\Delta Q_\beta = \xi \frac{\Delta E}{E_0} Q_{\beta 0} \tag{11}$$

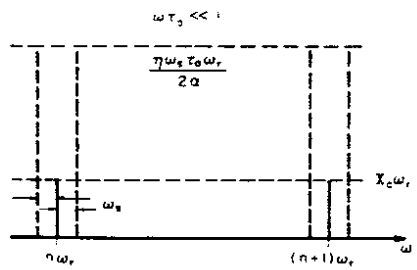

1361188-014

Figure 2: The low frequency spectrum from a closed orbit error and energy oscillations.

where $Q_{\beta 0}$ is the tune of a nominal energy particle. Let $\psi_\beta(t)$ denote the phase of the betatron oscillation at time t. The time rate of change of ψ_β is

$$\frac{d\psi_\beta}{dt} = \omega_r Q_\beta = \omega_r Q_{\beta 0}(1 + \xi \frac{\Delta E}{E_0}) = \omega_\beta + \omega_\xi \frac{d\tau}{dt} . \tag{12}$$

Equations (II.14) and (II.15) have been used. $\omega_\beta = Q_{\beta 0}\omega_r$, and $\omega_\xi = \omega_\beta\xi/\alpha$. Integrating

$$\psi_\beta(t) = \psi + \omega_\beta t + \omega_\xi \tau = \psi + \omega_\beta t + \omega_\xi \tau_a \cos(\omega_s t + \phi) . \tag{13}$$

ϕ is the phase of the synchrotron oscillation at $t = 0$, and ψ is a constant of integration related to the phase of the betatron oscillation at $t = 0$

$$\psi = \psi_\beta(t=0) - \omega_\xi \tau_a \cos\phi \quad . \tag{14}$$

The dipole moment is

$$d(t) = A_\beta e^{j\psi_\beta(t)} \sum_{n=-\infty}^{\infty} \delta[t - nT - \tau_a \cos(\omega_s nT + \phi)] \quad . \tag{15}$$

and the Fourier transform is

$$D(\omega) = A_\beta e^{j\psi} \sum_{n=-\infty}^{\infty} \exp\{j(\omega_\beta - \omega)nT\} \times$$

$$\exp\{[(\omega_\beta - \omega) + \omega_\xi]\tau_a \cos(\omega_s nT + \phi)\} \quad . \tag{16}$$

Both arrival time modulation and the dependence of ψ_β on τ contribute to the argument of the second exponential. By analogy to the discussion for longitudinal motion, both can be expected to contribute to the spectral envelopes. Using the Bessel function sum (eq. (II.11)) and the Poisson sum rule (eq. (II.5))

$$D(\omega) = \omega_r A_\beta e^{j\psi} \sum_{k=-\infty}^{\infty} (j)^k e^{jk\phi} J_k\{\tau_a(\omega_\beta - \omega + \omega_\xi)\} \times$$

$$\sum_{n=-\infty}^{\infty} \delta[\omega - (n\omega_r + \omega_\beta - k\omega_s)] \quad . \tag{17}$$

The index k enters into the spectral frequencies and the envelopes. For a fixed k, the lines are offset from the rotation harmonics by $\omega_\beta - k\omega_s$; this is independent of ξ. The envelopes have most of the properties discussed for the longitudinal. They are Bessel functions centered at $\omega = \omega_\beta + \omega_\xi \equiv \omega_\xi$ rather than $\omega = 0$. Chromaticity shifts the envelopes away from $\omega = 0$. This is illustrated for $k = 0$ in figure 3a. The envelope shifts to positive or negative frequency depending on ξ. The envelope width is determined by τ_a. $J_0(z)$ has a central maximum at $z = 0$ and the first minima at $z = \pm 2.4$. In terms of frequencies the maximum is at ω_ξ, and the first minima are at $\omega = \omega_\beta + \omega_\xi \pm 2.4/\tau_a$. Figure 3b shows this for two values of τ_a. When $k \neq 0$, the first maxima of the envelope occur at

$$\omega \sim \omega_\beta + \omega_\xi \pm \frac{k}{\tau_a} . \tag{18}$$

Figure 3c shows this for $k = 1$, $\omega_\xi = -1$ and two values of τ_a; the two envelopes are centered at $\omega = -1$ but the structures have different scales.

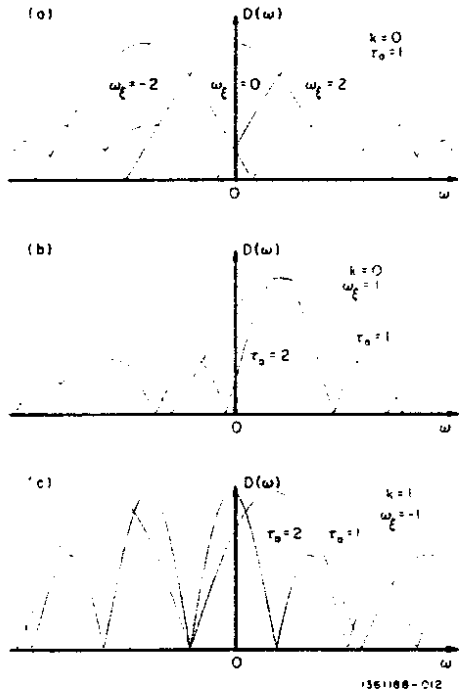

Figure 3: Spectral envelopes. a) k = 0 for different chromaticities, b) k = 0 for different synchrotron oscillation amplitudes, c) k = 1 for different synchrotron oscillation amplitudes.

Consequences of these chromaticity effects are that synchrotron sidebands of the betatron frequency can appear near $\omega \sim 0$, and positive and negative frequency lines need not have equal amplitude. In figure 4a $\xi = 0$; the only lines near $\omega \sim 0$ are betatron lines ($k = 0$). At $\omega \sim 2.4/\tau_a$ the betatron lines are small ($J_0(\omega\tau_a) \sim 0$), and the synchrotron sidebands for $k = \pm 1, \pm 2$, and ± 3 can be seen. The figure was drawn for $q_\beta = 0.38$; consequently the left-hand sets of lines are the positive frequency lines and the right-hand set the negative frequency ones. They have equal amplitudes because $\xi = 0$.

In figure 4b $\omega_\xi = 2$, and the spectrum is strikingly different: 1) the betatron lines at low frequency have smaller amplitudes, 2) there are synchrotron sidebands at low frequency, 3) there are betatron lines at $\omega\tau_a \sim 2.4$, and 4) the positive and negative frequency lines have equal amplitudes at $\omega \sim 0$, but at $\omega\tau_a \sim 2.4$ they have different amplitudes. The last of these follows because the positive and negative frequency lines come from $\omega_+ = n_+\omega_r + \omega_\beta - k\omega_s$ ($n_+ \sim k\omega l/\omega_r$) and $\omega_- = n_-\omega_r + \omega_\beta - k\omega_s$ ($n_- \sim -k\omega l/\omega_r$), respectively. For $\omega \sim 0$, $n_+ = 0$, $n_- = -1$, and the Bessel functions do not change significantly for this small a frequency difference. At $\omega\tau_a = 2.4$ the arguments of the Bessel functions are different ($\omega_+ - \omega_- = 4.8/\tau_a$), and as a result, the amplitudes of the lines are unequal.

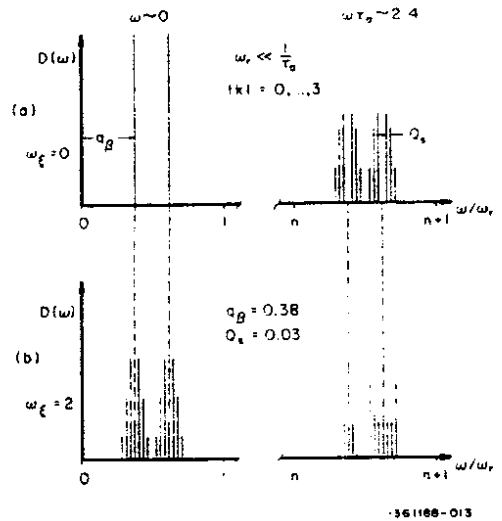

Figure 4: Spectral lines near $\omega \sim 0$ and $\omega \sim 2.4/\tau_a$ for a) zero chromaticity and b) $\omega_\xi = 2$.

C. Multiple Particles: Introduction

The discussion will concentrate on betatron oscillations. In analogy with eq. (II.16) the beam is described by a 4-dimensional charge density, ρ_4, defined by

$$\rho_4(\tau_a, \phi, A_\beta, \psi)\,\tau_a d\tau_a d\phi A_\beta dA_\beta d\psi = \text{charge in phase space volume } \tau_a d\tau_a d\phi A_\beta dA_\beta d\psi \qquad (19)$$

where τ_a = the synchrotron oscillation amplitude,
ϕ = the synchrotron oscillation phase at $t = 0$,
A_β = the betatron oscillation amplitude,
ψ = eq. (14) gives the phase of the betatron oscillation at $t = 0$ in terms of ψ.

The beam signal is given by multiplying the single particle signal, eq. (17), by ρ_4 and integrating over phase space.[1] Schottky noise and collective effects are considered in detail.

D. Schottky Noise

This treatment parallels section II.D. The particles move independently, and, as a consequence, the average charge density doesn't depend on ϕ and ψ. In addition, the betatron and synchrotron amplitudes of a particle are assumed to be independent of each other. The average charge density is

---

1. Note that ρ_4 could have been written as a function of $\psi_\beta(t = 0)$ rather than ψ, but the above choice is more natural because ψ enters directly into the phase of eq. (17). Using $\psi_\beta(0)$ would introduce another Bessel function sum!

$$\bar{\rho}_4 = \frac{1}{4\pi^2}\,\rho_s(\tau_a)\rho_\beta(A_\beta). \tag{20}$$

When eq. (17) is multiplied by this and the integral over ψ performed, the result is zero. The signals from individual particles cancel on average because of their different betatron phases.

As in the longitudinal, fluctuations from the average lead to Schottky noise. For P particles the charge density is

$$\rho_4 = q\sum_{p=1}^{P}\delta(\tau_a-\tau_{ap})\,\delta(\phi-\phi_p)\,\delta(A_\beta-A_{\beta p})\,\delta(\psi-\psi_p) \tag{21}$$

where τ_{ap},... are the coordinates of particle p. The dipole moment at $\omega = n\omega_r + \omega_\beta - k\omega_s$ is

$$D_{nk}(\omega) = q\omega_r\sum_{p=1}^{P}A_{\beta p}\exp[j(\psi_p+k\phi_p+k\pi/2)]\,J_k(\tau_{ap}(\omega_\xi+\omega_\beta-\omega)) \;. \tag{22}$$

The mean value, given by averaging over all samples of P particles, is zero. This holds even for k = 0 because the phase depends on the betatron oscillation phase.

The square of the rms dipole moment is

$$\begin{aligned}\langle D_{nk}^2(\omega)\rangle &= \frac{1}{2}\langle D_{nk}(\omega)\,D_{nk}^*(\omega)\rangle \\ &= \frac{q^2\omega_r^2}{2}\left\langle\sum_{p=1}^{P}\sum_{s=1}^{P}A_{\beta p}A_{\beta s}\exp(j(\psi_p-\psi_s))\exp(jk(\phi_p-\phi_s))\;\times\right. \\ &\qquad \left. J_k(\tau_{ap}(\omega_\xi+\omega_\beta-\omega))\,J_k(\tau_{as}(\omega_\xi+\omega_\beta-\omega))\right\rangle \;.\end{aligned} \tag{23}$$

The average phase factor equals zero unless p = s; this removes one of the sums

$$\langle D_{nk}^2(\omega)\rangle = \frac{q^2\omega_r^2}{2}\left\langle\sum_{p=1}^{P}A_{\beta p}^2\;J_k^2(\tau_{ap}(\omega_\xi+\omega_\beta-\omega))\right\rangle \;. \tag{24}$$

Equation (24) shows that the rms fluctuation is proportional to the typical betatron amplitude and the square root of the number of particles.

Following section II.D

$$\left(\langle D_{nk}^2(\omega)\rangle\right)^{1/2} = \omega_r\left(\frac{q}{2}\int_0^\infty\rho_s(\tau_a)\,J_k^2(\tau_a(\omega_\xi+\omega_\beta-\omega))\,\tau_a d\tau_a\int_0^\infty\rho_\beta(A_\beta)\,A_\beta^3 dA_\beta\right)^{1/2}. \tag{25}$$

For a Gaussian beam with bunch length σ_τ and width σ_β,

$$\bar{\rho}_4 = \frac{Q}{4\pi^2}\frac{1}{\sigma_\tau^2\sigma_\beta^2}\;\exp[-\tau_a^2/2\sigma_\tau^2 - A_\beta^2/2\sigma_\beta^2] \;. \tag{26}$$

the integral over A_β equals $2\sigma_\beta^2$. Performing the integral over τ_a^2

$$\left(\langle D_{nk}^2(\omega)\rangle\right)^{1/2} = \omega_r q\sigma_\beta\left(P\;\exp[-(\omega_\xi+\omega_\beta-\omega)^2\sigma_\tau^2]\,I_k[(\omega_\xi+\omega_\beta-\omega)^2\sigma_\tau^2]\right)^{1/2}. \tag{27}$$

The envelopes are centered at $\omega \sim \omega_\xi$ and have broad maxima at $k\omega - \omega_\xi k\sigma_\tau \sim k$ (figure 5).

---

2. I. S. Gradshteyn and I. M. Ryshik, Table of Integrals, Series, and Products (New York: Academic Press, 1965), eq. 6.633.2.

Most of this result is just what would be expected from a simple statistical argument. The mean position of the beam is being measured with P independent particles, and, as with any measurement, the error in the mean is $1/\sqrt{P}$ times the rms spread of a single measurement - σ_β in this case. Therefore, the expected signal should be equal to that from a charge Pq with a displacement $\sigma_\beta/\sqrt{P}$. This argument doesn't give the dependences on frequency, bunch length, and chromaticity.

Typically P is measured with a beam current monitor, and σ_τ is measured with a longitudinal detector. Given these, the rms dipole moment can be used to measure transverse properties of the beam including the fractional part of the tune, the beam width, and the chromaticity. The rms signal voltage is

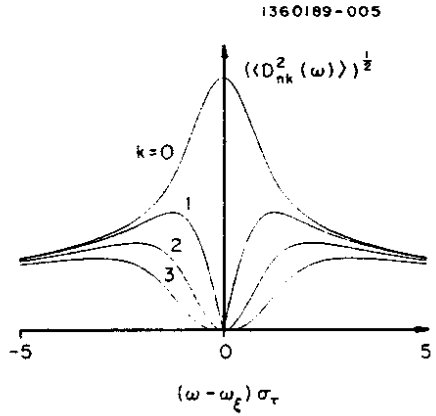

Figure 5: The rms dipole moment for k = 1, 2, 3.

$$\tilde{V}_{rms}(\omega) = S_\Delta\left(\langle D_{nk}^2(\omega)\rangle\right)^{1/2} \tag{28}$$

where S_Δ is the detector sensitivity. The signal levels are low even with a high sensitivity detector. In addition, there can be large, unwanted signals from closed orbit errors. These have different frequencies, but they can overload electronics, and they must be removed by filtering. From these considerations, the situation to analyze is that of a detector/electronics system with a relatively narrow frequency range (less than ω_r) centered at an appropriately chosen frequency.

In the following discussion examples are based on experience at the Tevatron when the parameters were approximately those in Table I. Some of the points above are illustrated in figure 6. Figure 6a shows a 1 MHz span centered at the peak response of the detector. The dominant signals are the rotation harmonics spaced at 47.7 kHz; they don't have equal amplitudes because there were three bunches in the machine. Figure 6b shows a 100 kHz span centered at the same frequency; the betatron lines can be seen but only because the motion is being stimulated by external excitation. Schottky signals would be 20 to 40 db lower in amplitude.

First consider betatron tune measurement (k = 0). Just as for a single particle, the signal frequency gives the fractional part of the tune, q_β

$$q_\beta = \frac{\omega}{\omega_r} - n, \quad\text{or}\quad q_\beta = n + 1 - \frac{\omega}{\omega_r} \tag{29}$$

where the frequency is in the range $n\omega_r \le \omega \le (n+1)\omega_r$. The ambiguity can be resolved by changing the tune in a known direction. The rms voltage is given by eqs. (27) and (28) with k = 0. This is plotted for the Tevatron parameters in figure 7. The signal voltage is 0.25 μV near $\xi - 0$. This corresponds to an rms motion of the mean position, $\sigma_\beta/\sqrt{P} = 3.4$ nm!

For comparison the Johnson Noise equals[3]

$$\tilde{V}_{noise}(\omega) \sim 2\pi(4kTR\Delta\nu_b)^{1/2} \;. \tag{30}$$

---

3. P. Horowitz and W. Hill, The Art of Electronics (Cambridge: Cambridge University Press, 1980), sect 7.10.

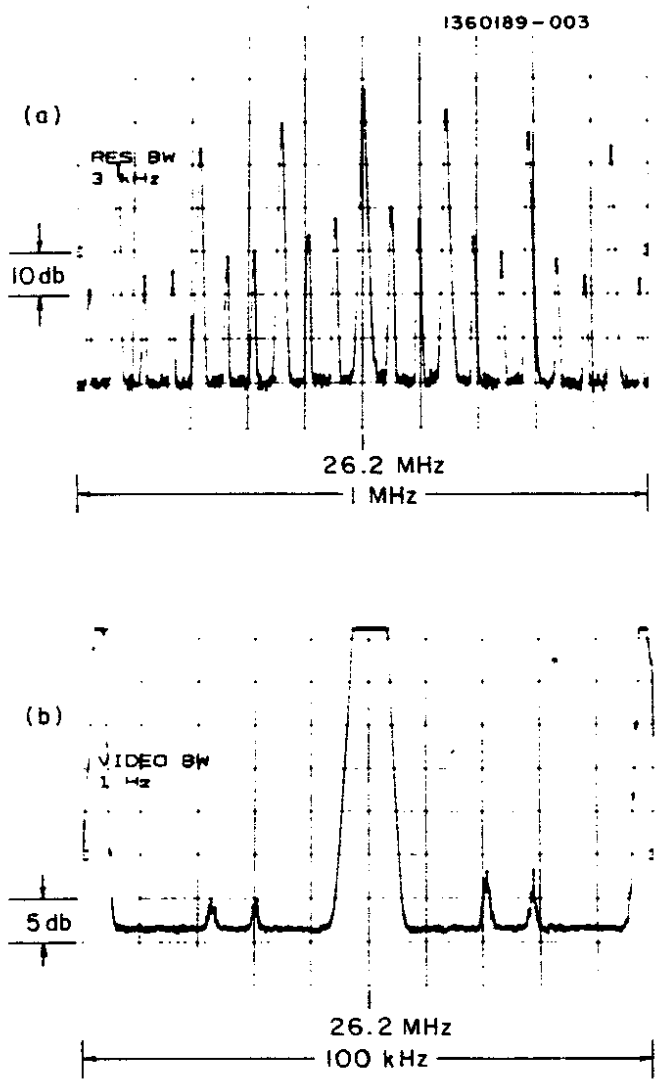

Figure 6: Tevatron beam signals; the detector was tuned to 26.2 MHz for these pictures.

Table I: Transverse Motion in the Tevatron Collider, 1987*

Betatron Tunes	Horizontal	$Q_\beta = 19.407$
	Vertical	$Q_\beta = 19.404$
Normalized Emittance		7×10^{-6} m
Beam Energy		E = 900 GeV
Emittance		7×10^{-9} m
β Functions at Detector Locations		100 m
Beam Sizes at Detector Locations		$\sigma_\beta = 0.84$ mm
Revolution Frequency		$\nu_r = 47.7$ kHz
Synchrotron Oscillation Frequency		$\nu_s = 37$ Hz
RMS Bunch Length		$\sigma_\tau = 1.4$ nsec
Momentum Compaction		$\alpha = 0.0030$
Number of Particles in a Single Bunch		$P = 6 \times 10^{10}$
	Detector/Electronics Properties	
Center Frequency		21.4 MHz
Frequency Range		15 kHz
Sensitivity		$S_\Delta = 27\ \Omega$/mm

* Related longitudinal parameters are given in Chapter II, Table I.

k is Boltzmann's constant, T is the absolute temperature,[4] R is the input impedance of the electronics, and $\Delta\nu_b$ is the measurement bandwidth. Choosing $\Delta\nu_b = 10$ Hz, the approximate spread of betatron frequencies, and $R = 50\ \Omega$ gives a noise voltage of 20 nV which is about a factor of ten below the signal level. It is difficult to reach the Johnson noise level for several reasons: i) the signal processing electronics introduces noise (although amplifiers with noise figures of only a few db are commercially available), ii) there is pickup at connectors, flanges and breaks in the outer conductor of signal cables, and iii) the combination of closed orbit signals and non-linearities in the filters can combine to generate intermodulation products.[5] The noise from these sources can be limited, but it requires careful work.

There is a spread of betatron frequencies caused by effects such as non-linearities leading to amplitude dependence of tune and the beam-beam interaction. The tune distribution can be measured by reducing the measurement bandwidth, $\Delta\nu_b$, below the betatron frequency spread. The rms dipole moment is given by eq. (27) with the P replaced by the number of particles in $\Delta\nu_b$; the change is analogous to that in eqs. (II.30) and (II.31). Near the peak of the tune distribution the fraction of particles is $\sim 4\Delta\nu_b/\sigma_\nu$ where σ_ν is the rms tune spread. The ratio of signal to Johnson noise is $(10kTR\sigma_\nu)^{-1/2}$ at the peak of the distribution and lower in the tails. Both the Schottky signal and the noise are statistical, and the signal-to-noise ratio affects the measurement time needed to see a meaningful signal.

The beam width follows directly from the signal amplitude through eq. (27). The principal uncertainty is whether that equation is the correct interpretation of the signals. It isn't if there are collective effects (section III.E) or if there is an external excitation of the beam. The latter was important in the initial running of the Tevatron collider. The beam size determined by eq. (27) was inconsistent with the size measured with flying wires. This led to the conclusions that the motion of the center-of-charge was substantially larger than $\sigma_\beta/\sqrt{P}$ and that there must be external excitations of the beam. A rapidly fluctuating 1 Gauss-mm magnetic field could explain the data. Ultimately, the RF system, abort kickers, and interaction region quadrupoles were found to be sources of excitation.[6]

---

4. $4kT = 1.62 \times 10^{-20}\ V^2/Hz\cdot\Omega$ at 293 K.
5. E. Hafner, IEEE Trans. on Sonics and Ultrasonics, SU-21, 220 (1974).
6. G. Jackson et al, "Luminosity Lifetime in the Tevatron", 1988 Rome Accelerator Conference.

It should be noted that such external excitation does not affect tune measurements. In fact, low level noise excitation of the beam is often used to "shake" the beam for rapid tune measurement.

The most direct way to measure the chromaticity is to vary the beam energy while keeping the magnetic fields fixed by changing the RF frequency. The change of tune with energy gives ξ (eq. (11))

$$\xi = \alpha \frac{\Delta Q_\beta / Q_{\beta 0}}{\Delta \nu_{RF} / \nu_{RF}} \quad . \qquad (31)$$

An alternative method is a measurement of the relative amplitudes of the synchrotron sidebands of the betatron frequency. Eq. (27) gives the rms signals at different sideband frequencies when the signal is due to Schottky noise. The relative moments are correct also if the beam is excited by externally applied noise, but the equation is incorrect if there are collective effects. Assume this is not the case. The amplitudes for the Tevatron are plotted in figure 7. Near $\xi = 0$ the only signals are at $\omega = n\omega_r + \omega_\beta$ ($k = 0$) and $\omega = n\omega_r \pm \omega_\beta \pm \omega_s$ ($k = \pm 1$). As $|\xi|$ increases more sidebands appear.

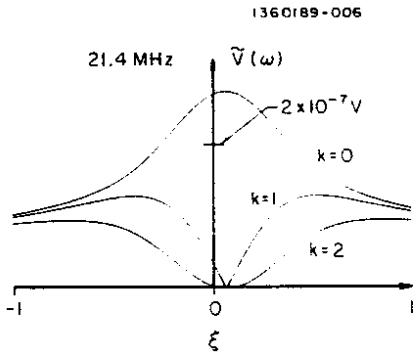

Figure 7: Tevatron signals at 21.4 MHz.

Figure 8 shows some data from the Tevatron taken when the beam was externally excited and both the horizontal and vertical betatron lines could be seen. The vertical $k = \pm 1$ lines are 3 to 4 db below the $k = 0$ line, and the $|k| = 2$ lines are barely visible; from figure 7 the chromaticity is $\xi_v \sim 0.4$ or $\xi_v \sim -0.3$. The beam would be unstable if the chromaticity were negative (the head-tail instability),[7] so $\xi_v \sim 0.4$. In the horizontal the $k = 0, \pm 1$, and ± 2 lines are clearly seen, and from the ratios of amplitudes the chromaticity is measured to be $\xi_h \sim 0.7$.

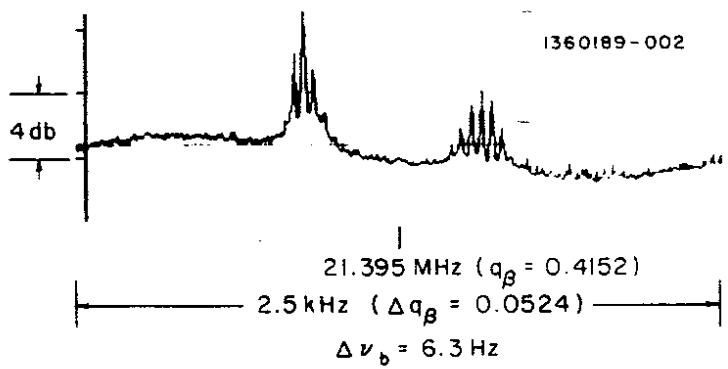

Figure 8: Vertical (on the left) and horizontal (on the right) transverse signals from the Tevatron.

7. C. Pellegrini, Nuovo Cimento LXIV, 447 (1969).
M. Sands, SLAC-TN-69-8 (SLAC, 1969).

E. Collective Effects

In this case particles do not move independently, and the beam develops phase space structure by interacting with the surrounding environment. The mechanism is closely related to that discussed in section II.E: 1) the beam generated dipole signal interacts with the environment (the transverse impedance of the accelerator) and produces deflecting wakefields, 2) these act back on the beam to modify the phase space distribution, 3) this changes the beam generated signal and the wakefields. The coherent modes are the solution of this eigenvalue problem.

The charge density at $t = 0$ (eq. (19)) is a periodic function of ϕ and ψ, and it can be expanded in a Fourier series in those angles

$$\rho_4(\tau_a, \phi, A_\beta, \psi) = \sum_{q,r} \chi_{qr} \exp\{j(q\phi + r\psi)\}; \quad q, r = -\infty, \ldots, \infty . \qquad (32)$$

The expansion coefficients are functions of τ_a and A_β. Multiplying eq. (17) by ρ_4 to get the dipole signal and performing the ψ integration gives

$$D(\omega) \propto \sum_r \int_0^{2\pi} d\psi \exp\{j\psi(r+1)\}. \qquad (33)$$

The integral equals zero unless $r = -1$, and, therefore, only that term has a dipole signal.

The transverse coherent modes have betatron amplitudes that are the same for all particles with the same synchrotron amplitude.[8] Using this and the result from eq. (33), ρ_4 is

$$\rho_4(\tau_a, \phi, A_\beta, \psi) = e^{-j\psi} \sum_{q=-\infty}^{\infty} \rho_q(\tau_a) \delta\{A_\beta - A_{\beta q}(\tau_a)\} e^{jq\phi}. \qquad (34)$$

This is the charge density for calculating the signals of coherent modes.

1. Approximate Picture: Begin with the approximation that the phase space structure is evolving slowly and the tunes aren't changed by wakefields. I.e. at a later time t an expression similar to eq. (34) could be written, the ρ_q's would differ by only a phase factor, $\exp\{j(\omega_\beta + \omega_s)t\}$, which accounts for the phase space motion of particles. The signal is given by multiplying eq. (17) by ρ_4 and integrating over phase space

$$D(\omega) \propto \sum_{\substack{q \\ n,k}} \int_0^{2\pi} d\phi \exp\{j\phi(k+q)\} \delta\{\omega - (n\omega_r + \omega_\beta - k\omega_s)\}. \qquad (35)$$

This integral equals zero unless $q = -k$. The ϕ periodicity determines the signal frequency; if $\rho_4 \sim \exp(jq\phi)$, the signal frequency is $\omega = n\omega_r + \omega_\beta + q\omega_s$.

The general result is

$$D(\omega) = \sum_{n,k} D_{nk}(\omega) \; \delta\{\omega - (n\omega_r + \omega_\beta + k\omega_s)\}$$

where (36)

$$D_{nk}(\omega) = 4\pi^2 \omega_r (j)^k \int_0^\infty \tau_a d\tau_a \rho_k(\tau_a) A_{\beta,-k}(\tau_a) J_k(\tau_a(\omega_\beta - \omega + \omega_s)).$$

The D_{nk}'s depend on the phase space structure, and that needs to be known to calculate the signal. This is in contrast to the Schottky case where there are no unknowns. The Bessel function in the integrand has the usual effect of correlating the periodicity in ϕ and the frequency range of the signal. As $|k|$ increases the signal shifts to higher values of $|\omega - \omega_\xi|$.

8. J. L. Laclare, 11th International Conference of High-Energy Accelerators (Basel: Birkhaeuser Verlag, 1980, edited by W. S. Newman), p. 526.

To show the qualitative features of this result assume i) the coherent eigenmodes are given by Hermite polynomials,[9] and ii) A_β is independent of τ_a. Begin with k = 0

$$\rho_0 \propto \exp\{-\tau_a^2/2\sigma_\tau^2\} \quad . \tag{37}$$

Substituting into eq. (36) and performing the integrals[10]

$$D_{n0}(\omega) \propto \exp\{-(\omega_\beta - \omega + \omega_\xi)^2\sigma_\tau^2/2\}. \tag{38}$$

D_{n0} is a Gaussian with an rms width of $1/\sigma_\tau$ centered at $\omega \equiv \omega_\xi$. This is similar to point being illustrated in figure 3b for a single particle. In both cases, ξ determines the center frequency and the longitudinal amplitude determines the width. However, in the present case the distribution of synchrotron amplitudes washes out the multiple zeros in figure 3b.

For |k| = 1

$$\rho_k \propto \tau_a \exp\{-\tau_a^2/2\sigma_\tau^2\} \quad . \tag{39}$$

and[11]

$$D_k(\omega) \propto (\omega_\beta - \omega + \omega_\xi)\exp\{-(\omega_\beta - \omega + \omega_\xi)^2\sigma_\tau^2/2\}. \tag{40}$$

This envelope has two maxima: one is at $\omega \equiv 1/\sigma_\tau + \omega_\xi$ and the other at $\omega \equiv -1/\sigma_\tau + \omega_\xi$. Eqs. (38) and (40) illustrate the second way that the longitudinal phase space structure affects the signal. In addition to giving the frequencies of the spectral lines ($\omega = n\omega_r + \omega_\beta + k\omega_s$), it determines the spectral envelope. As |k| increases, the peaks in the envelope move to higher values of $|\omega - \omega_\xi|$. Whether this is higher or lower $|\omega|$ depends on ω_ξ; for example, for $\omega_\xi \sim 1/\sigma_\tau$, the k = 0 signal is centered at $\omega \sim 1/\sigma_\tau$ while one peak of the k = 1 envelope is at a lower frequency, $\omega \sim 0$ (the other one is at $\omega \sim 2/\sigma_\tau$).

The result from eq. (33), that only the r = -1 term in eq. (32) has a dipole signal, leads to the chromaticity effects that have been shown formally. They can be understood intuitively by considering the dipole moment (eq. (1)). Using eq. (13) the transverse displacement of a chunk of charge at $\tau = 0$ is

$$x(\tau) = A_\beta \exp\{j\psi_\beta(0)\} = A_\beta \exp\{j(\psi + \omega_\xi\tau)\} \quad . \tag{41}$$

The dipole moment is given by multiplying $x(\tau)$ by ρ_4 and integrating over phase space. The goal is to calculate $d(\tau)$, and this is easiest if eq. (II.15) is used to switch from polar to Cartesian coordinates. Doing this

$$d(\tau) = e^{j\psi}\sum_k \int d\varepsilon\, \rho_k(\tau_a) A_\beta(\tau_a) \exp\{j(\omega_\xi\tau + k\phi)\} \quad . \tag{42}$$

where $\phi = \tan^{-1}(\varepsilon/\tau)$ and $\tau_a^2 = \tau^2 + \varepsilon^2$. The dipole moment depends on τ through the longitudinal structure of the bunch and the phase shift of the transverse displacement along the bunch. The latter is proportional to ξ. The dipole signal depends on the interference between these two terms.

---

9. These arise naturally for a bunch with a Gaussian distribution.
   G. Besnier, Thesis, Univ. Rennes (1978).
   B. Zotter, CERN/ISR-TH/80-03, (CERN, 1980).
10. I. S. Gradshteyn and I. M. Ryshik, Table of Integrals, Series, and Products (New York: Academic Press, 1965), eq. 6.631.7.
11. Ibid. eq. 6.631.4.

The dipole moment for k = 0 is plotted in figure 9a using ρ_0 from eq. (37).[12] The transverse displacement varies turn-by-turn, but on any given turn its variation along the bunch depends on ξ. When $\xi = 0$, it is independent of τ, and the dipole signal has the longitudinal profile of the bunch with its characteristic time scale of σ_τ. When $\xi \neq 0$, the transverse displacement depends on τ, and, as the figure shows, the signal has a shorter time scale. That corresponds to the shift of the spectrum away from $\omega = 0$.

The same plot is repeated for k = 1 in figure 9b. When $\xi = 0$, the transverse displacement is independent of τ; the dipole moment changes sign as τ goes through zero because of the longitudinal structure of the bunch. When $\xi \neq 0$, the dipole moment is complicated due to the combination of longitudinal structure and dependence of transverse displacement on τ. The signal does have a non-zero average value which can be seen by looking at it turn-by-turn (figure 9c). This low frequency signal arises from the interference between the two contributions to the τ dependence, and in the formal result (eq. (40)) it is the shift of one of the peaks to $\omega \sim 0$.

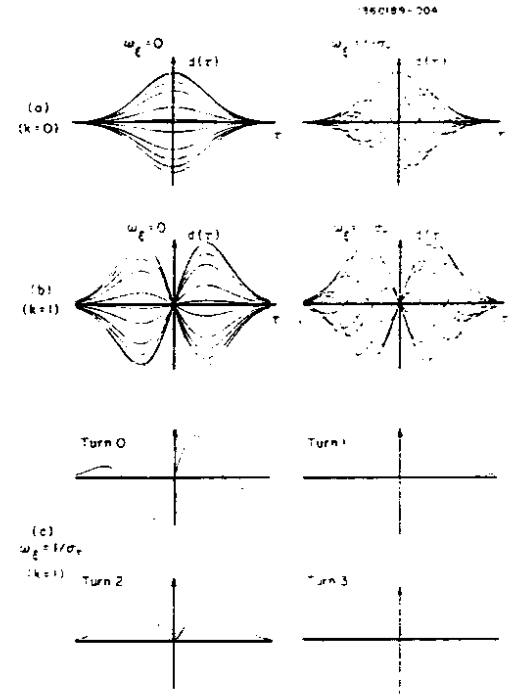

Figure 9: The dipole moment on successive turns for a) ρ_0 given by eq. (37) and b) ρ_1 given by eq. (39). c) The k = 1 signal when $\omega_\xi = 1/\sigma_\tau$ on 4 successive turns. $q_\beta = 0.38$.

---

12. $d(\tau)$ on turn N is given by multiplying eq. (42) by $\exp(j\omega_\beta NT)$.

2. Coherent Tune Shifts: Growth, damping, and frequency shifts due to wakefields can be accounted for with a treatment similar to that in section II.E.2. The charge density at time t is expanded in a Fourier series in ϕ and an appropriate basis in the radial coordinate, τ_a

$$\rho_4(t) = \sum_{q,p} \rho_{qp}(\tau_a)\,\delta\{A_\beta - A_{\beta q}(\tau_a)\}\exp\{j[(\omega_\beta+\Delta\Omega_{qp}+\omega_s)t+\omega_\xi\tau+q\phi]\} \quad . \quad (43)$$

The dipole signal can be calculated for each term in eq. (43); that signal multiplied by the transverse impedance gives the deflecting fields that act back on the beam. The frequency shifts and modes are the eigenvalues and eigenvectors, respectively, of the resultant eigenvalue problem.

The detailed formulation starting with the Vlasov equation is contained in the reviews referenced in section II.E. A summary of results is:

1. A perturbation approach to the Vlasov equation leads to an integral equation involving a convolution (over frequency) of the dipole signal and the transverse impedance.
2. The $\Delta\Omega_{qp}$'s are proportional to the beam current and the transverse impedance weighted by the frequency spectrum of the mode. The mode spectrum depends on the ϕ periodicity, the radial (τ_a) structure, and chromaticity; therefore, the frequency shifts are different for each mode and depend on ξ.
3. The $\Delta\Omega_{qp}$'s are complex. The real part, $\Delta\omega_{qp} = \mathrm{Re}(\Delta\Omega_{qp})$, changes the betatron frequency from ω_β to $\omega_\beta + \Delta\omega_{qp}$. The imaginary part, $\Gamma_{qp} = -\mathrm{Im}(\Delta\Omega_{qp})$, can lead to growth or damping. Landau damping and/or radiation damping can prevent instabilities.
4. The imaginary part of the transverse impedance is the component of the deflecting field in phase with the displacement. This component shifts the betatron frequency and determines $\Delta\omega_{qp}$.
5. The real part of the transverse impedance is the component of the deflecting field that is 90° out of phase with the displacement. It can add or remove energy from the betatron oscillation and determines Γ_{qp}.
6. At low current signal frequencies depend on q, the longitudinal phase space periodicity, as $\omega = n\omega_r + \omega_\beta + q\omega_s$. As the beam current increases the frequencies shift away from these values. When $|\Delta\Omega_{qp}| \sim \omega_s$, modes with different periodicity can couple; this leads to the "fast head-tail" instability which has a large growth rate.

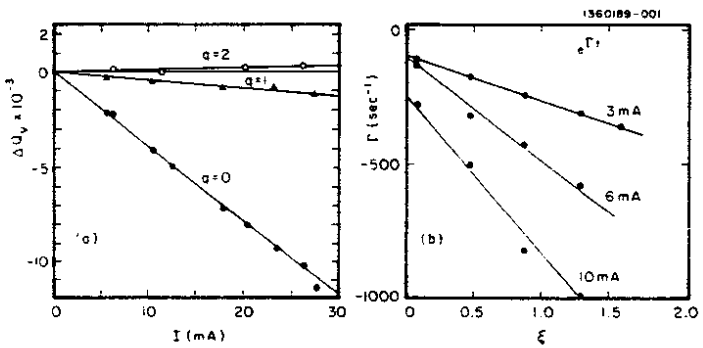

Figure 10: Collective effects in CESR. a) frequency shifts with beam current.[13] b) damping of coherent motion excited by "pinging" the beam.[14]

---

13. D. H. Rice et al, IEEE Trans. Nucl. Sci. NS-28, 2446(1981).
14. L. E. Sakazaki, private communication.

Some of these points are illustrated with data from CESR in figure 10. The data in figure 10a show betatron tune shifts for modes with q = 0, 1, and 2. These measurements were made at low frequency, $\omega - q\beta\omega_r$, and positive chromaticity. The beam was driven with a "shaker magnet" (an external field); the drive frequency tracked the measurement frequency. The azimuthal periodicity, q, was determined by the signal frequency, and different radial modes could not be distinguished. These data illustrate point 2 above. The signal spectra are different for these modes, and, therefore, the tune shifts are unequal because they are determined by the transverse impedance in different frequency ranges.

The data in figure 10b show coherent damping as a function of chromaticity. These data were taken by giving the beam an impulse and measuring the decay time constant of the coherent signal with a tuned receiver centered at $\omega = q\beta\omega_r$ (the q = 0 frequency). The spectrum shifts as ξ is changed, and this affects the frequency range over which the impedance is sampled. If the lines in figure 10b are extrapolated to $\xi < 0$, Γ would be positive and there would be an instability. This is the head-tail instability that was discovered at Frascati and Orsay and interpreted by Pellegrini and Sands.

F. Multiple Particles: Summary

This is a summary of the previous two sections.

Schottky Noise

Spectrum	A comb of sidebands at integer multiples of the synchrotron frequency offset from the rotation harmonics by ω_β, $\omega = n\omega_r + \omega_\beta + k\omega_s$, n, k = $-\infty,\ldots,\infty$.
Envelopes	1. The overall normalization is known; it is proportional to the square root of the number of particles and the typical betatron amplitude. (eq. 24))
	2. If $\rho_s(\tau_a)$ and $\rho_\beta(A_\beta)$ are known, the frequency dependence of the rms dipole signal is known. There are no relative or absolute uncertainties. (eq. (25))
	3. For a general charge density the dipole signal is given by the convolution of charge density with J_k^2. The envelope is centered at $\omega = \omega_\xi + \omega_\beta$. (eq. (25))
	4. For a Gaussian bunch the envelopes are centered at $\omega \sim \omega_\xi$. There are broad maxima at $\lvert\omega - \omega_\xi\rvert \sim k/\sigma_\tau$. (eq. (27) and figure 5)
Measurement	1. The sideband frequency gives the fractional part of the betatron tune. (eq. (29)).
	2. The signal amplitude gives the beam size and/or can be used to diagnose excitation of the beam.
	3. The shift of tune with RF frequency gives the chromaticity. (eq. (31))
	4. The relative amplitudes of sidebands measures the chromaticity. (figure 7)

Collective Effects

Spectrum	A collective mode with periodicity in longitudinal phase space given by $\exp(jq\phi)$ produces signals at $\omega = n\omega_r + \omega_\beta + q\omega_s$. (eq. (35)) In addition, there is a frequency shift $\Delta\omega$ that depends on the azimuthal and radial structure of the mode in longitudinal phase space.
Envelopes	1. The minimum detectable signal is that due to Schottky noise.
	2. The overall normalization is not known. (eq. (36))
	3. The frequency dependence is determined by the τ_a dependence of the coherent mode. Signals from coherent modes with high periodicity in longitudinal phase space tend to be strong at high frequencies (eq. (36))
Measurement	1. A signal above the Schottky noise level is an indication of a coherent mode. The displacement of the sideband from the betatron frequency gives the azimuthal structure of the mode.
	2. Frequency shift as a function of current gives qualitative information about the accelerator impedance.

IV. Beam Detectors

A. Introduction[1]

For a relativistic beam, the line density of the image current flowing on the vacuum chamber wall equals the line density of the beam (with an overall minus sign because it's an image current)

$$i_w(t) = -i_b(t) \quad ; \quad I_w(\omega) = -I_b(\omega) \ . \qquad (1)$$

This follows from the Lorentz contraction of the electromagnetic fields of a relativistic particle. From a circuit point-of-view the image current is as close as you can get to an ideal current source - the image current will flow through any impedance placed in its path. A beam detector (or any other object) with impedance $Z(\omega)$ can be analyzed as a circuit with a current source driving the impedance (figure 1). If Z is a beam detector which is sensitive to longitudinal motion and voltage V_{out} is produced across load R, the detector's longitudinal sensitivity is defined as

$$S(\omega) = \frac{V_{out}(\omega)}{I_b(\omega)} \ . \qquad (2)$$

1360189-011

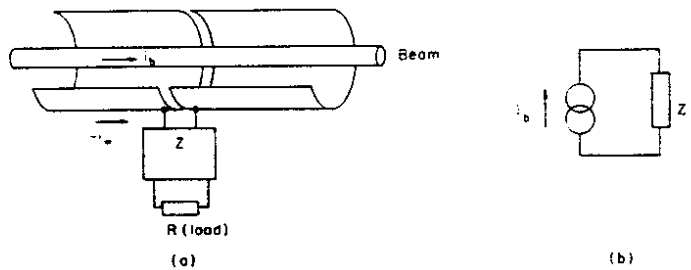

Figure 1: a) The beam and wall currents. b) The equivalent circuit.

1360189-009

The distribution of image current around the beam pipe circumference depends on beam pipe geometry and the position of the beam. Figure 2 shows an example of a detector that measures the transverse displacement of the beam. The impedance, Z, and load resistor, R, are connected between the two sides of the detector. The transverse sensitivity of the detector in terms of the voltage V_{out} across R is

$$S_\Delta(\omega) = \frac{V_{out}(\omega)}{D(\omega)} \ . \qquad (3)$$

$D(\omega)$ is the dipole moment which was discussed extensively in chapter III.

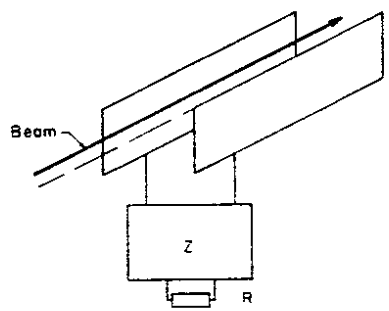

Figure 2: A transverse beam detector.

Two specific detectors are discussed in the following sections.

---

1. This approach comes from D. Boussard, "Schottky Noise and Beam Transfer Function Diagnostics", Proc. CERN Accel. School, Advanced Accel. Physics, CERN 87-03 (CERN, 1987).

B. The SPS Wideband Wall Current Pick-Up[2]

The detector is a gap in the beam pipe (figure 1a). There is a closed metallic chamber around the gap which provides shielding, gives a DC current path, and, for this particular detector, is the vacuum enclosure. The latter could have been avoided by using a ceramic gap, but this was decided against for reasons discussed below. The wall current flows through a parallel combination of the gap capacitance, C, the measuring resistor, R, and the impedance of the shielding box, Z. The voltage developed across the gap is

1360189-007

$$V(\omega) = I_b(\omega) \frac{1}{j\omega C + \frac{1}{R} + \frac{1}{Z}} \ . \qquad (4)$$

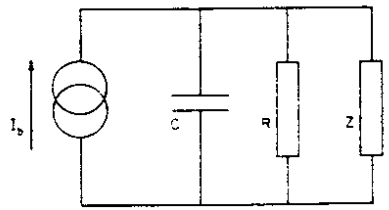

The shielding box is inductive at low frequencies; the cutoff is $\omega_{low} = R/L$. The gap capacitance determines the high frequency cutoff; it would equal $\omega_{high} = 1/RC$ if Z were purely inductive. The beam pipe-shielding box structure can have resonances, and these will modify the high frequency behavior.

Some comments about the design criteria are: 1) it pays to increase the inductance to reduce the low frequency cutoff, 2) the gap capacitance should be decreased to raise the high frequency cutoff, 3) attention must be paid to resonances and other aspects of the high frequency behavior of the structure, 4) R and Z should be distributed around the circumference of the beam pipe to avoid beam position sensitivity. Usually there are other factors such as available space and cost which strongly influence a design. These are impossible to include in a general way, so the choice was made to describe a particular detector, the SPS wall current pick-up. Figure 3 is a schematic.

The inductance can be increased by inserting ferrite between the beam pipe and shielding box,[3] but ferrite becomes lossy at high frequencies and gives a poorly characterized high frequency performance. Instead, the shielding box (#1 in figure 3) and beam pipe (#2) were configured like the conductors of a coaxial line with a characteristic impedance $Z_0 = 25\ \Omega$. Absorptive material (#20) placed between the conductors produces a matched load. The line is terminated above ~ 10 MHz, and the reflection coefficient is less than 0.13 for frequencies from 300 MHz to above 4 GHz. The low frequency inductance is about 0.25 μH. The coaxial line-absorber design involved bench measurements of different absorber materials and configurations; the original references discuss these in detail.

The gap was chosen to be 2 mm long (detail drawings at bottom of figure 3) which was a compromise between low capacitance and mechanical constraints. With this gap and an 83 mm diameter, 1.5 mm thick beam pipe, the gap capacitance is 7 pF. The design specification was for $\nu_{high} > 4$ GHz, so the parallel combination of R and Z_0 must be less than 5.75 Ω. A vacuum rather than ceramic gap was selected because ceramic would have increased the capacitance and needed a thin metallic coating to prevent charge build-up. A factor in this decision was that the RF absorber could be conditioned to have good vacuum properties without affecting its RF properties.

The signal was coupled out at eight points equally spaced around the circumference: this removed sensitivity to beam position. Stripline (50 Ω, figure 3, detail A) was used between the gap and output connectors; without this the series inductance of the lead determined the high frequency response. The output powers were added with a 50 Ω hybrid, and with the hybrid output terminated in 50 Ω, each of the eight signal points has a 50 Ω resistance.

---

2. T. P. R. Linnecar, IEEE Trans. Nucl. Sci. NS-26, 3409(1979).
   T. Linnecar, CERN-SPS/ARF/78-17 (CERN, 1978).
3. For example, G. C. Schneider, Proc. 1987 IEEE Particle Accelerator Conference (New York: IEEE Publishing Services, 1987, edited by E. R. Lindstrom and L. S. Taylor), p. 664.

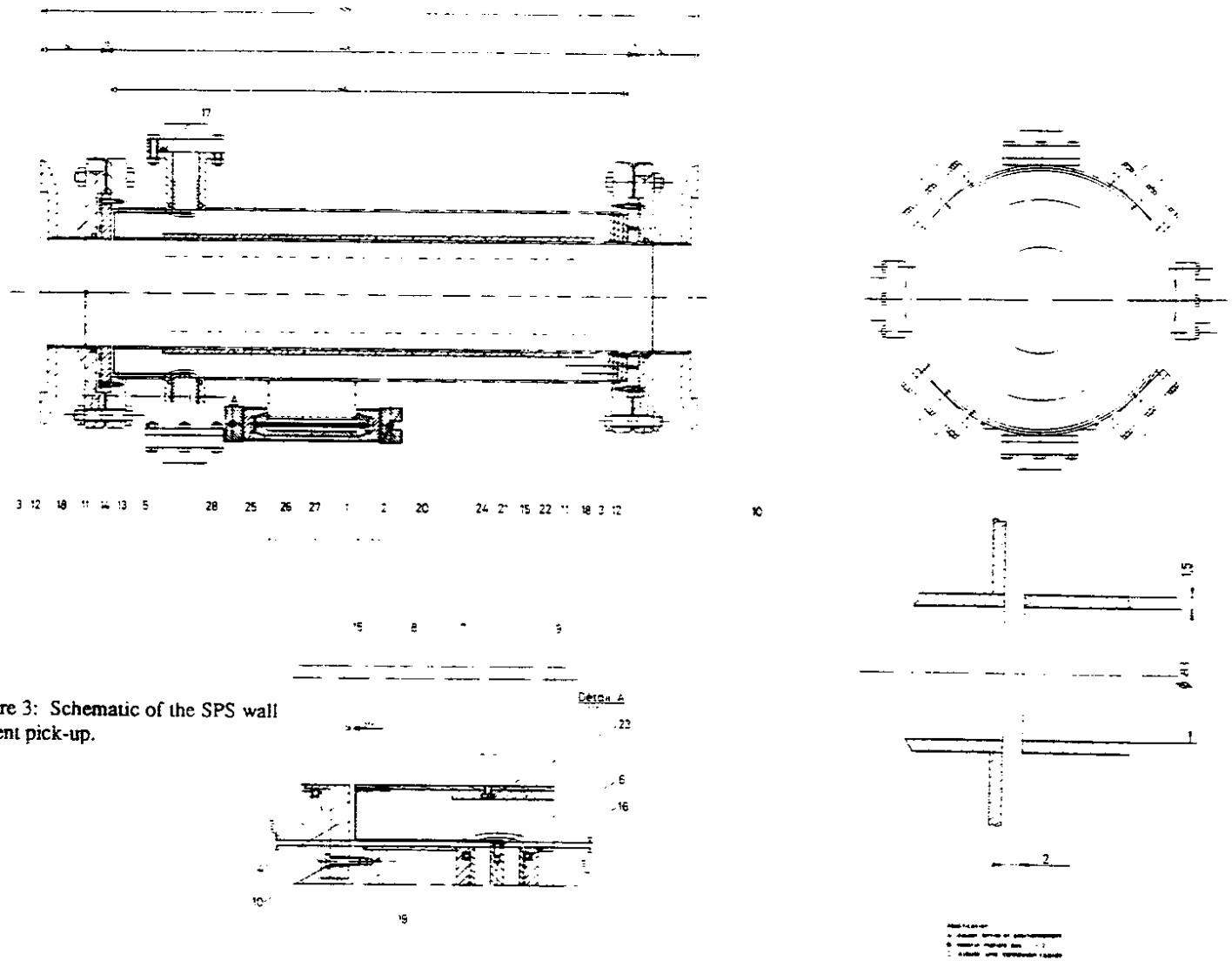

Figure 3: Schematic of the SPS wall current pick-up.

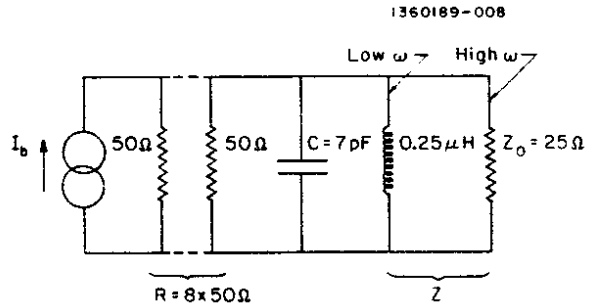

Figure 4: The equivalent circuit of the SPS detector.

The equivalent circuit for this detector is shown in figure 4. At intermediate frequencies where the capacitance and inductance can be ignored, $i_b/5$ flows through Z_0 and $i_b/10$ flows through each of the 50 Ω resistors. The power generated in each resistor is

$$P = i^2 R = (i_b/10)^2 \times 50\ \Omega = i_b^2 \times 0.5\ \Omega . \tag{5}$$

The hybrid adds power; there is a loss, K = 1.12, in the hybrid. The output power is

$$P_{out} = \frac{8}{K} \times i_b^2 \times 0.5\ \Omega , \tag{6}$$

and the output voltage and sensitivity are

$$V_{out} = i_b \times (50 \times 3.565)^{1/2}\Omega ; \quad S = 13.4\ \Omega . \tag{7}$$

The frequency response of the detector was measured under several conditions. In all cases ν_{low} = 4.2 to 4.4 MHz. Looking directly at one of the eight outputs with all the others terminated ν_{high} = 4.4 GHz. When the eight signals are combined in the hybrid, ν_{high} = 3.1 GHz; the hybrid was limiting the frequency response. When the signal is run through 120 m of high quality cable to beam diagnostic area, ν_{high} = 2.0 GHz; this is consistent with specified cable attenuation. This loss can be avoided by placing the analyzing instrument, a spectrum analyzer or sampling head, close to the detector. Of course, the instrument must be under remote control and have remote readout, but with the IEEE bus this has become considerably easier than it used to be.

This wideband detector is used at the SPS for pulse measurements. How would it do with Schottky signals? Using $I_b(\omega)$ = 4 nA (figure II.4) and S = 13.4 Ω, the signal is 54 nV; this a factor of ten above the Johnson noise (eq. (III.30)) for $\Delta\nu_b$ = 1 Hz. The detector could be used for Schottky measurements.[4]

C. The Tevatron Transverse Beam Detector[5]

The goals were to design and build a high sensitivity detector that could be used for tune measurements with Schottky noise. The detector concept, shown in figure 2, is based on earlier work by Linnecar and Scandale at the SPS.[6] It is a set of parallel plates with impedance Z connected

4. The SPS has a narrowband Schottky detector with S = 385 Ω (CERN-SPS/ARF/78-17).
5. D. Martin et al, to be presented at the 1989 IEEE Particle Accelerator Conference.
6. T. Linnecar and W. Scandale, IEEE Trans. Nucl. Sci. NS-28, 2147 (1981).

between them. Z has several elements; the main one is a loosely coupled transformer. Figure 5 is a detailed schematic of the detector.

1. **Background:** Let $I_L(\omega)$ and $I_R(\omega)$ denote the wall currents on the left- and right-hand plates at the upstream end of the detector. They depend on the transverse displacement of the beam and the fraction of the total wall current that flows on the plates[7]

$$I_{R,L}(\omega) = -I_b(\omega)\left(\frac{2}{\pi}\tan^{-1}(\zeta) \pm \frac{2x}{g}\,\frac{\zeta}{1+\zeta^2}\right) ; \quad \zeta = \tanh(\pi w/4g) . \tag{8}$$

In this equation g is the plate separation, w is the plate height, x is the displacement towards the right-hand plate, and the + (-) sign applies for I_R (I_L). When $w/g \geq 1$, $\zeta/(1+\zeta^2) \sim 1/2$. Only the difference current will develop a voltage across Z; at the upstream end it is

$$I_u(\omega) = I_L(\omega) - I_R(\omega) = D(\omega)\,\frac{4}{g}\,\frac{\zeta}{1+\zeta^2} . \tag{9}$$

At the downstream end of the detector the current equals

$$I_d(\omega) = -\exp(-j\omega l_p/v_b)\, I_u(\omega) . \tag{10}$$

There is an overall minus sign because current flows off the plates, and the phase shift accounts for the time it takes the beam to travel the length of the plates (v_b is the velocity of the beam and l_p is the length of the plates).

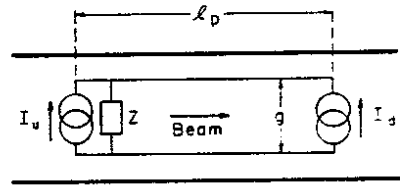

The plates together with the surrounding enclosure form a transmission line with characteristic impedance Z_0. Assume, for the purpose of discussion, that Z has been connected at the upstream end of the detector as shown above. The upstream current source sees Z in parallel with the impedance of the transmission line terminated terminated in an open circuit. The voltage from the upstream current source is[8]

$$V_u = \frac{I_u}{Y_u} ; \quad Y_u = \frac{1}{Z} + \frac{j}{Z_0}\tan(\omega l_p/v_s) \tag{11}$$

where v_s is the signal phase velocity. From now on take $v_b = v_s = c$, and let $\theta = \omega l_p/c$ (θ is the length of the plate in units of phase). In terms of θ

$$V_u = I_u Z\,\frac{e^{2j\theta}+1}{e^{2j\theta}+1 + \frac{Z}{Z_0}(e^{2j\theta}-1)} . \tag{12}$$

7. A. G. Ruggiero, Fermilab p̄ Note 199, (FNAL, 1982).
8. Reference Data for Radio Engineers (Indianapolis: Howard W. Sams & Co, 1977), chap. 24.

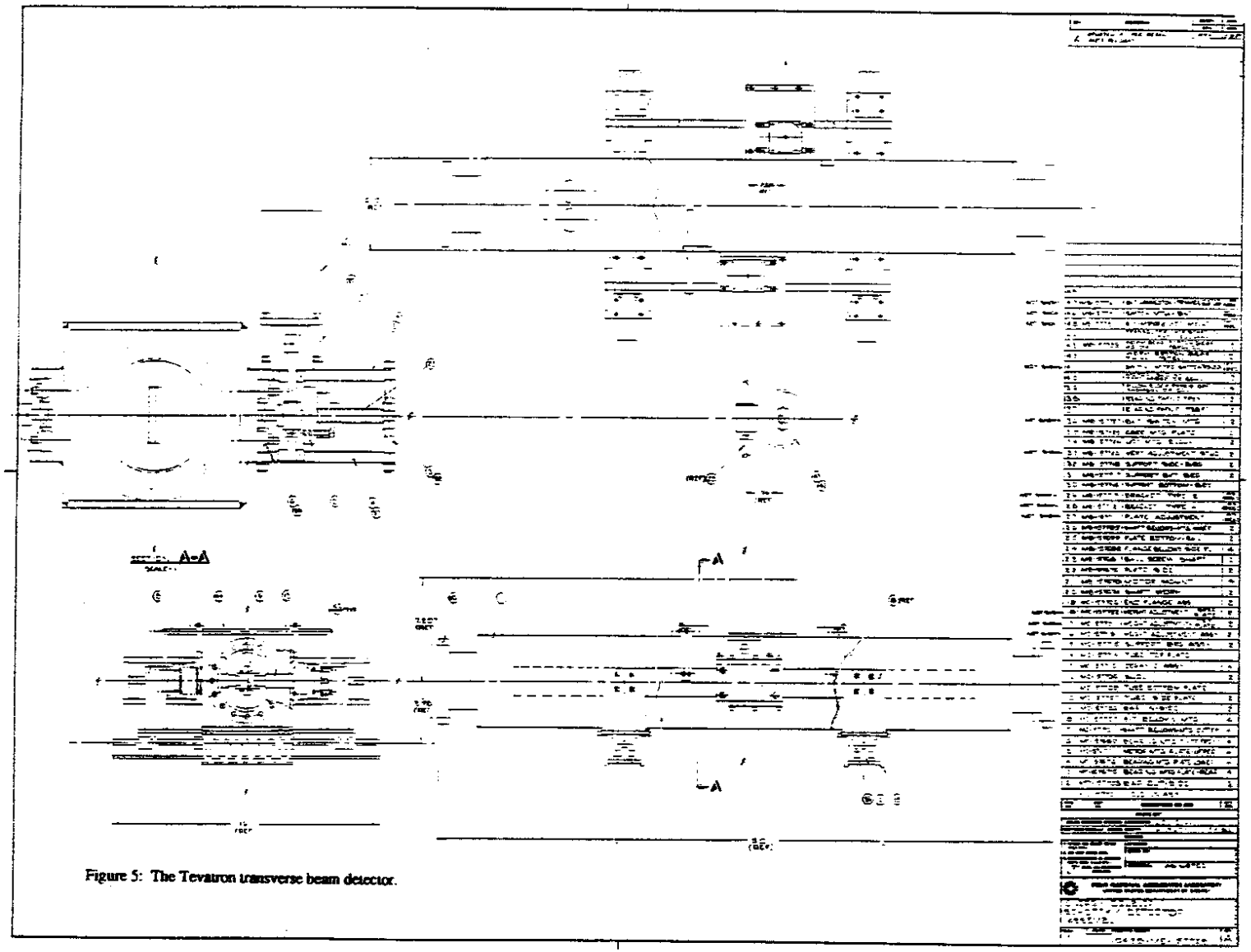

Figure 5: The Tevatron transverse beam detector.

The voltage across Z from I_d can be calculated by transforming Z to downstream end, calculating the voltage there, and transforming back to the upstream end; the result is

$$V_d = I_d Z \frac{2e^{j\theta}}{e^{2j\theta}+1+\frac{Z}{Z_0}(e^{2j\theta}-1)} = -I_u Z \frac{2}{e^{2j\theta}+1+\frac{Z}{Z_0}(e^{2j\theta}-1)} . \qquad (13)$$

Adding them together

$$V = V_u + V_d = I_u Z_0 \frac{Z(e^{2j\theta}-1)}{Z_0(e^{2j\theta}+1)+Z(e^{2j\theta}-1)} . \qquad (14)$$

When $\theta << 1$, eq. (14) becomes

$$V = I_u j\theta \frac{Z_0 Z}{Z_0 + j\theta Z} . \qquad (15)$$

The transmission line capacitance per unit length, C', and characteristic impedance are related as $Z_0 = 1/C'c$. Using this eq. (15) becomes

$$V = I_u j\theta \left(\frac{1}{Z} + j l_p C' \omega \right)^{-1} . \qquad (16)$$

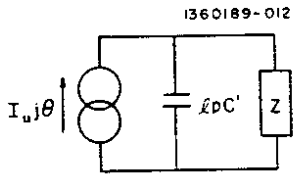

The circuit is a current source $I_u j\theta$ driving the parallel combination of Z and capacitor $l_p C'$.

The complete circuit is in figure 6a. It is a resonant circuit with the signal transformer-coupled out to the load, R. The principal element of Z is the transformer which is modelled by the parallel combination of shunt resistor, R_s, ideal inductor, L, and an ideal n-turn transformer. Z has two parallel capacitors also. C_s is the stray capacitance between leads (ideally $C_s = 0$), and C_v is a variable capacitor that is adjusted to keep the resonant frequency fixed when the gap is changed.

The resonant frequency is $\omega_{res} = (LC)^{-1/2}$ ($C = l_p C' + C_s + C_v$). The impedances of L and C cancel at resonance, and when R is transformed to the primary the circuit is that in figure 6b. R_s and n can be expressed in terms of the Q's of the circuit which are measurable quantities. Without the load the circuit Q would be the "unloaded Q", Q_0, and with the load it is the "loaded Q", Q_L

$$Q_0 = \omega_{res} R_s C ; \quad Q_L = \omega_{res} \left(\frac{1}{R_s} + \frac{n^2}{R} \right)^{-1} C . \qquad (17)$$

Combining these two equations the transformer ratio is

$$n^2 = \frac{1}{Q_L} \left(1 - \frac{Q_L}{Q_0} \right) R\omega_{res} C . \qquad (18)$$

The final circuit is in figure 6c; the current source $I_u j\theta$ is driving a resistor $Q_L/\omega_{res}C$. The output voltage is $V_{out} = nV$. Using eqs. (3) and (9) the sensitivity is

$$S_\Delta = \frac{4 l_p \zeta}{cCg(1+\zeta^2)} \left(Q_0 R\omega_{res} C \left(\frac{Q_L}{Q_0} \left[1 - \frac{Q_L}{Q_0} \right] \right) \right)^{1/2} . \qquad (19)$$

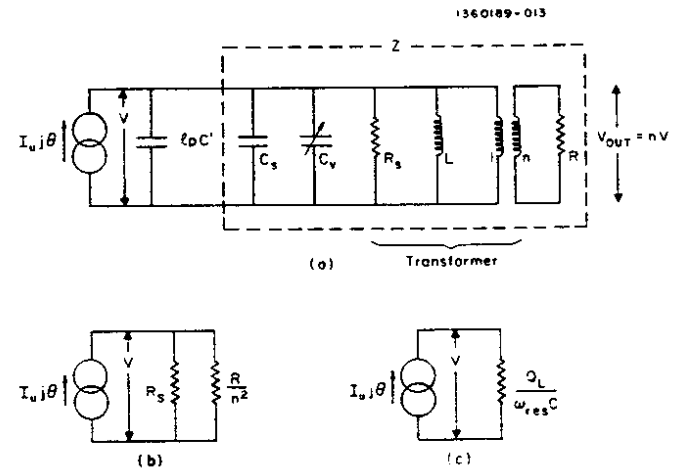

Figure 6: a) The equivalent circuit for the Tevatron detector. The circuit at resonance b) in terms of R_s and R, and c) in terms of Q_L.

Make some approximations. When $w/g \geq 1$ and C_v, $C_s << l_p C'$, the coefficient equals $2/(cC'g)$. If the plates are far from the surrounding enclosure and fringe fields ignored, $C' = \varepsilon_0 w/g$. S_Δ is a maximum when $Q_L/Q_0 = 1/2$; then

$$S_\Delta = \left(\frac{Q_0 R Z_0 \omega_{res}}{c} \frac{l_p}{wg} \right)^{1/2} \qquad (20)$$

where $Z_0 = 377\ \Omega$ is the characteristic impedance of free space. Q_0 should be as large as possible consistent with the range of tune to be measured, $Q_0 \leq \omega_{res}/\omega_r$, the gap and plate height should be small, and the plates should be long.

2. The Tevatron Detector: With this background the Tevatron detector, shown in figure 5, is discussed. The detector frequency was chosen by the availability of components. A filter is needed to attenuate rotation harmonics (figure III.6), and relatively inexpensive crystal filters can be purchased "off-the-shelf" at 10.7 and 21.4 MHz. The latter frequency equals 448.51 ν_r, and with a 21.4 MHz filter that has a 15 kHz bandwidth a tune range $0.35 < q_B < 0.65$ can be measured. This covers the Tevatron operating point, so $\omega_{res} = 2\pi \times 21.4$ MHz was chosen.

The gap and plate height should be small (with $w/g \geq 1$) for high sensitivity. However, the gap must be large at injection time and during energy ramps so the aperture won't be restricted. The solution is to make the plates moveable. The translation mechanism should keep the plates parallel to avoid unnecessary loss of aperture; $l_p = 1$ m was chosen as a compromise between increasing the sensitivity ($S_\Delta \propto \sqrt{l_p}$) and minimizing mechanical problems.

The transformer primary is an air-core inductor made of several turns of refrigerator tubing.[9] In early models of the detector it was four turns of 1/4" tubing wound with a 1/2" pitch on a 1.96"

---

9. Refrigerator tubing is ideal; it is easy to wind and retains its shape when the winding form is removed.

diameter form: this gave $L \sim 0.65\ \mu H$ and $Q_0 \sim 410$. The transformer secondary is a loop that intercepts some of the flux of the primary. The "turns-ratio" and inductance were adjusted empirically. First, the gap was reduced to the minimum desired value, $g = 10$ mm, and C_v was set equal to zero. L was adjusted by making small changes in the inductor length until $\nu_{res} = 21.4$ MHz. Second, the turns-ratio was adjusted by removing load R and measuring the input impedance at what would normally be the signal output using a vector impedance meter. R_s transformed to the secondary equals

$$n^2 R_s = \frac{Q_0}{Q_L}\left[1 - \frac{Q_L}{Q_0}\right] R \ . \qquad (21)$$

The area and/or position of the secondary were adjusted until the impedance at 21.4 MHz equaled R; then $Q_L = Q_0/2$.[10]

The detector parameters are given in Table I. The spectra in figures III.6 and III.8 were taken with (unintentional) external excitation of the beam and high sensitivity wasn't required. The gap was $g = 22$ mm, and $S_\Delta = 27\ \Omega$/mm. With g gap reduced to the design value, $g = 10$ mm, the sensitivity would be $S_\Delta = 59\ \Omega$/mm.

Table I: Tevatron Transverse Beam Detector, 1987

Resonant frequency		$\nu_{res} = 21.4$ MHz
Plate length		$l_p = 1.0$ m
Plate height		$w = 2.54$ cm
Capacitance		$C = 85$ pF
Inductance		$L = 0.65\ \mu H$
Unloaded Q		$Q_0 = 410$
Loaded Q		$Q_L = 205$
Load resistance		$R = 50\ \Omega$
	$g = 22$ mm	$g = 10$ mm
Plate capacitance/unit length	$C' = 25$ pF/m	$C' = 55$ pF/m
Sensitivity	$S_\Delta = 27\ \Omega$/mm	$S_\Delta = 59\ \Omega$/mm

The sensitivity can be doubled and the signals from counterrotating beams separated by adding signals from two detectors that are one-quarter wavelength, $\lambda/4$, apart. Let detector #1 be $\lambda/4$ from detector #2 and let #1 be upstream of #2 for protons and downstream of #2 for anti-protons. Assuming equal detector sensitivities[11] $V_2(\omega) = V_1(\omega)\exp(-j\pi/2)$ for protons, and $V_2(\omega) = V_1(\omega)\exp(j\pi/2)$ for anti-protons. If the signal from #1 is added to the signal from #2 after being delayed by a cable with a 90^0 phase shift, the proton and anti-proton signals are

$$V_p(\omega) = V_1(\omega)e^{-j\pi/2} + V_2(\omega) = 2V_1(\omega)e^{-j\pi/2}$$
$$V_{\bar{p}}(\omega) = V_1(\omega)e^{-j\pi/2} + V_2(\omega) = V_1(\omega)\{e^{-j\pi/2} + e^{j\pi/2}\} = 0 \qquad (22)$$

The anti-proton signals have interfered destructively, and the proton signals have interfered constructively giving a signal which is twice that of a single detector. If V_2 is delayed rather than V_1, the $\bar{p}$ signal doubles while the p signal cancels.

---

10. It is necessary to compensate for the self inductance of the secondary loop by working at the "detuned short" position. See E. L. Ginzton, Microwave Measurements (New York: McGraw-Hill Book Company, 1957), sect. 9.3.
11. In practice the sensitivities aren't equal, but attenuators can compensate for this.

3. Signal Processing: For some purposes it is adequate to filter the signal to remove the rotation harmonics, amplify it, and measure the resultant spectrum directly. However, the resolution bandwidths of spectrum analyzers useful at 21.4 MHz are typically $\Delta\nu_b \geq 10$ Hz, and this limits measurements of tune distributions.

It is possible to get much higher resolution by mixing the signal down to a frequency range where an audio spectrum analyzer can be used. This is illustrated schematically for the Tevatron detector in figure 7. The detector signal is filtered, amplified, and mixed with the signal from a local oscillator running at 448 ν_r. If the signal frequency is ν ($\nu \sim 21.4$ MHz), the mixer output frequencies are $\nu + 448\nu_r$ (~ 43 MHz) and $\nu - 448\nu_r$. The latter is well within the frequency range of Fast Fourier Transform signal analyzers. These have resolution bandwidths which are a percentage of the frequency span; 0.25% is typical. This signal processing arrangement is simple and has some flexibility; for example, the filter and local oscillator frequencies can be changed to study coupled bunch effects. This does require a custom made filter, and delivery can be long and costs high.

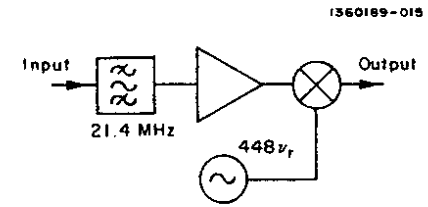

Figure 7: Frequency translation by mixing.

It is easiest to use a frequency synthesizer as the local oscillator, but this has the disadvantage of not tracking the revolution frequency. ν_r changes by about 1 Hz ($\Delta\nu_r/\nu_r \sim 2\times10^{-5}$) as the Tevatron ramps from injection, 150 GeV, to collisions, 900 GeV. If the local oscillator frequency was fixed and q_β was constant during the energy ramp, the output frequency of the circuit in figure 7 would change by 430 Hz. This large a frequency change makes it difficult to measure tune changes during the ramp.

This problem can be avoided if the local oscillator frequency is derived from the RF as shown in figure 8. Phase-locked loops are used to derive local oscillator signals at $371\nu_r$ (~ 17.7 MHz) and $77\nu_r$ (~ 3.67 MHz). The outputs from the first stage of mixing are at $\nu + 371\nu_r$ and $\nu - 371\nu_r$ where ν is the signal frequency. The higher frequency signal is removed by the 3.7 MHz filter, and the lower frequency signal is mixed giving outputs at $\nu - 294\ \nu_r$ and $\nu - 448\nu_r$. The former is filtered out and the latter is sent to the audio spectrum analyzer. With this solution changes in the signal frequency are changes in tune, and it is easy for the operators to measure tune changes during the ramp.

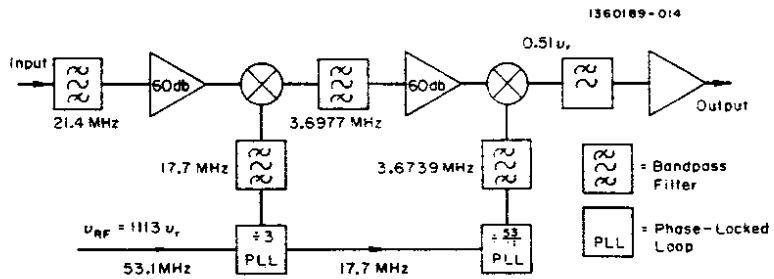

Figure 8: The Tevatron tune receiver with local oscillators locked to the RF.[12]

The End

---

12. D. Martin and R. Shafer, private communication.